M 2018

U.PORTO
FEUP FACULDADE DE ENGENHARIA
UNIVERSIDADE DO PORTO

PRODUCTION OF NANOPARTICLES AND MICROPARTICLES USING THE NETMIX TECHNOLOGY

CLÁUDIA CRISTINA FERREIRA DE ALMEIDA

DISSERTAÇÃO DE MESTRADO APRESENTADA
À FACULDADE DE ENGENHARIA DA UNIVERSIDADE DO PORTO EM
ENGENHARIA QUÍMICA

Master in Chemical Engineering

Production of nanoparticles and microparticles using the NETmix technology

A Master's dissertation

of

Cláudia Cristina Ferreira de Almeida

Developed within the course of dissertation

held in

Associate Laboratory LSRE-LCM

SRE CM *ASSOCIATE LABORATORY*
LABORATORY OF SEPARATION AND REACTION ENGINEERING
LABORATORY OF CATALYSIS AND MATERIALS

Supervisors: **Prof. José Carlos Lopes**

Yaidelin J. Alves Manrique, PhD

U.PORTO
FEUP FACULDADE DE ENGENHARIA
UNIVERSIDADE DO PORTO

Departamento de Engenharia Química

July 2018

Agradecimentos

Para que este trabalho fosse bem-sucedido, contei com o apoio e incentivo de diversas pessoas, pelo que sinto a necessidade de lhes agradecer.

Ao Prof. José Carlos Lopes, pela forma como me orientou, pela atenção, disponibilidade e valor das suas opiniões.

À Doutora Yaidelin Manrique, pela constante prontidão em ajudar, por me dar o à vontade para discordar (mesmo quando me faltava a razão) e por todas as ideias e opiniões que muito acrescentaram a este projeto.

À Prof. Madalena Dias, que esteve sempre presente durante este percurso, pela oportunidade e por todo o apoio prestado.

Ao Prof. Joaquim Faria, pelo auxílio na caracterização físico-química do material.

A todo o *Mixing group*, em especial, à Andreia Ribeiro e à Catarina Moreira com quem tive o prazer de trabalhar mais de perto e que facilitaram a minha integração neste novo ambiente.

À Isabel Fernandes e à Margarida Duarte, que estiveram presentes dia após dia nestes últimos meses. Obrigada pelas memórias e momentos partilhados.

Ao Fábio Teixeira, pelo apoio incondicional e paciência infindável. A tua constante força foi essencial para o término deste trabalho.

À minha família, que lida comigo desde sempre e nunca reclamou (muito). À minha irmã, que é a versão pequena de mim e, por isso, me entende melhor que ninguém. À minha mãe, que sempre faz o impossível para que eu seja feliz. Ao meu pai, que será sempre um exemplo de força e de pessoa.

O meu sentido agradecimento a todos.

Este trabalho foi financiado por: Projeto POCI-01-0145-FEDER-006984 – Laboratório Associado LSRE-LCM – financiado pelo Fundo Europeu de Desenvolvimento Regional (FEDER), através do COMPETE2020 – Programa Operacional Competitividade e Internacionalização (POCI) e por fundos nacionais através da Fundação para a Ciência e a Tecnologia I.P.

Abstract

Nano and microtechnology are currently fields of great relevance, so much that the estimated value for its global market is expected to exceed one billion dollars by 2018. Calcium carbonate ($CaCO_3$), a natural and abundant mineral, is known in the form of three anhydrous crystalline polymorphs and has a wide range of applications. Its global demand is expected to reach 98.7 million metric tons by 2020 and one of the most important aspects in an industrial process of production of calcium carbonate is the control of the crystallization (since the properties of the product will vary depending on the composition of the polymorphs). Thus, two types of studies were carried out: the first consisted in semi-batch experiments where the particles of $CaCO_3$ produced were stored under different conditions and its stability studied over time; next, the NETmix reactor was used for the continuous production of $CaCO_3$ and the influence of some process variables on the final product was analysed.

In terms of the stability of the product over time, recrystallization occurred by the end of one week when the particles were stored in a suspension of distilled water. For a storage solution of both a hydrophobic and a hydrophilic compound (sodium oleate and sodium citrate, respectively) no recrystallization was verified in that period. A solution of sodium oleate stabilized the particles for, at least, 16 weeks and sodium citrate, although not as effective, also improved the particles' stability. This study also allowed to conclude that lower temperatures slowed recrystallization and that a twice more concentrated solution of sodium citrate was more effective in preventing recrystallization than a less concentrated solution. In the NETmix experiments, it was seen that, due to the mixing dynamics of the device, it was necessary to add the dispersant to the reactants (for recrystallization not to occur inside the reactor) and that the tested reaction temperatures had no effect on the produced particles. In the sodium citrate experiments, it was shown that less than four layers of dispersant were not enough to prevent recrystallization and that higher Reynolds numbers produced smaller clusters. Yet, when this number increased significantly (from 400 to 1500), it was verified a modification of the morphology of the formed particles. Sodium oleate experiments were not conclusive and were possibly compromised by an increase of the reactants' viscosity upon the addition of the dispersant, which could have lowered the Reynolds number below its critical value.

A preliminary economic assessment of a production plant of calcium carbonate with a maximum capacity of 600 $kg \cdot h^{-1}$ was made. It was concluded that a suspension of 17 % w/w of calcium carbonate must be sold at 5.4 $€ \cdot kg^{-1}$ for the investment to be returned in 5 years.

Keywords (theme): nanoparticles, microparticles, calcium carbonate, NETmix technology

Resumo

A área da nano/microtecnologia assume atualmente grande relevo, sendo estimado que o seu valor de mercado exceda um bilião de dólares até 2018. O carbonato de cálcio ($CaCO_3$), mineral natural e abundante, é conhecido na forma de três polimorfos cristalinos e apresenta uma vasta gama de aplicações. Um aspeto essencial na sua produção é o controlo da cristalização, visto que as propriedades do produto vão variar dependendo da composição dos polimorfos, e é estimado que a sua procura mundial atinja os 98,7 milhões de toneladas métricas até 2020. Assim, dois tipos de estudos foram efetuados: primeiro realizaram-se experiências *semi-batch*, armazenando as partículas de $CaCO_3$ produzidas sob diferentes condições e estudando a sua estabilidade ao longo do tempo; de seguida, utilizou-se o reator NETmix para a produção em contínuo e foi verificada a influência de certas variáveis processuais no produto final.

Relativamente à estabilidade do produto, observou-se a recristalização das partículas ao final de uma semana quando armazenadas numa suspensão de água destilada. Para uma solução de armazenamento de um composto hidrofóbico (oleato de sódio) ou hidrofílico (citrato de sódio), não foi verificada a recristalização durante esse período. A solução de oleato de sódio estabilizou as partículas durante, pelo menos, 16 semanas e o citrato de sódio, apesar de não tão eficaz, também melhorou a estabilidade das mesmas. Estas experiências permitiram também concluir que temperaturas inferiores retardam a recristalização e que uma solução de citrato de sódio com o dobro da concentração é mais eficaz a evitar a recristalização do que uma solução menos concentrada. Nas experiências efetuadas no NETmix, verificou-se que, devido à dinâmica de mistura do reator, era necessário adicionar os dispersantes aos reagentes (para a recristalização não ocorrer dentro do reator) e que as temperaturas de reação testadas não tiveram efeito significativo no produto obtido. Nas experiências com citrato de sódio, verificou-se que menos de quatro camadas de dispersante não eram suficientes para prevenir a recristalização e que números de Reynolds mais elevados produziam aglomerados menores. Contudo, quando este número aumentou significativamente (de 400 para 1500), foi verificada uma modificação na morfologia das partículas. As experiências com oleato de sódio não foram conclusivas, tendo sido possivelmente enviesadas pelo aumento da viscosidade dos reagentes aquando da adição de dispersante (o que poderá ter feito com que o número de Reynolds diminuísse para um valor abaixo do crítico).

Foi realizada uma análise económica preliminar a uma instalação de produção de carbonato de cálcio com capacidade máxima de 600 $kg \cdot h^{-1}$. Concluiu-se que a suspensão de 17 % m/m de carbonato de cálcio teria de ser vendida a 5,4 $€ \cdot kg^{-1}$ para que o investimento fosse recuperado em 5 anos.

Palavras Chave (Tema): nanopartículas, micropartículas, carbonato de cálcio, tecnologia NETmix

Declaration

I hereby declare, on my word of honour, that this work is original and that all non-original contributions were properly referenced with source identification.

Cláudia Cristina Ferreira de Almeida

July 2018

Contents

List of Figures

List of Tables

Notation and Glossary

a_m	area occupied by a molecule of nitrogen (0.162 nm^2 at -196 °C)	nm^2
C	molar concentration	$\mathrm{mol} \cdot \mathrm{L}^{-1}$
C_{BET}	parameter of the BET model	-
d	NETmix channels' diameter	mm
D	NETmix chambers' diameter	mm
I	ionic strength	$\mathrm{mol} \cdot \mathrm{L}^{-1}$
K_{sp}	solubility product constant	$\mathrm{mol}^2 \cdot \mathrm{L}^{-2}$
L	length	m
m	mass	g
MW	molecular weight	$\mathrm{g} \cdot \mathrm{mol}^{-1}$
n	number	-
n_m^a	monolayer capacity	$\mathrm{mol} \cdot \mathrm{g}^{-1}$
N	number of molecules	-
N_A	Avogadro's constant (6.022x10^{23})	mol^{-1}
P	pressure	Pa
P_0	maximum pressure	Pa
Q	mass flow rate	$\mathrm{kg} \cdot \mathrm{h}^{-1}$
r	radius	nm
Re	Reynolds number	-
S	surface area	m^2
S_{BET}	BET surface area	$\mathrm{m}^2 \cdot \mathrm{g}^{-1}$
T	temperature	°C
$TPSA$	topological polar surface area	nm^2
$\bar{v}$	average velocity	$\mathrm{m} \cdot \mathrm{s}^{-1}$
V	volume	m^3
V^a	adsorbed volume of nitrogen	$\mathrm{cm}^3_{\mathrm{PTN}} \cdot \mathrm{g}^{-1}$
V_m^a	volumetric capacity of the monolayer	$\mathrm{cm}^3_{\mathrm{PTN}} \cdot \mathrm{g}^{-1}$

Greek Letters

2θ	angle between two fringe spacings	°
α	number of layers	-
δ	fringe spacing	Å
ε_r	dielectric constant	-
μ	viscosity	$\mathrm{Pa} \cdot \mathrm{s}$
ρ	density	$\mathrm{kg} \cdot \mathrm{m}^{-3}$
ω	NETmix channels' depth	mm
ζ	zeta potential mean value	mV

Indexes

c	crystal
disp	dispersant
h	hydraulic
$\mathrm{h}', \mathrm{k}, \ell$	Miller indexes
reac	reactants
sp	solubility product

List of Acronyms

ACC	Amorphous Calcium Carbonate
APEA	Aspen Process Economic Analyzer
BET	Brunauer-Emmett-Teller
DP	Diffraction Pattern
EDS	Energy Dispersive Spectroscopy
FTIR	Fourier-Transform Infrared Spectroscopy
GCC	Ground Calcium Carbonate
INL	International Iberian Nanotechnology Laboratory
LCM	Laboratory of Catalysis and Materials
LDV	Laser Doppler Velocimetry
LSRE	Laboratory of Separation and Reaction Engineering
MW	Molecular Weight
PCC	Precipitated Calcium Carbonate
PIDS	Polarization Intensity Differential Scattering
PMG	Polymer Mediated Growth
PP	Polypropylene
PVC	Polyvinyl Chloride
RI	Refractive Index
SEM	Scanning Electron Microscopy
TAPPI	Technical Association of the Pulp and Paper Industry
TEM	Transmission Electron Microscopy
TPSA	Topological Polar Surface Area
XRD	X-Ray Diffraction

1 Introduction

Nano and microtechnology are currently fields of great relevance. Microtechnology has become crucial to several areas, including computer technology [1], and nanotechnology finds applications in the electronic, chemical and space industries, as well as in medicine and health care [2]. Areas such as materials and manufacturing, energy, biotechnology, information technology, national security and drug delivery also constitute promising fields of application for nanotechnology [3, 4]. In fact, the magnitude of both areas is such that the global market for the commercialization of micro-nanoproducts and systems was estimated to exceed one billion dollars by 2018 [5].

Examples of breakthrough products in the market include the Apple iPod (containing sub 100 nm elements in its memory chips), Canola Active Oil (a cholesterol-reducing nano-encapsulated oil from Shemen Industries), ArcticShield polyester socks from ARC Outdoors (with 19 nm silver particles that kill fungus) and Intel products (with 45 nm linewidth transistors) [5].

In general, the distinction between nanostructures and microstructures can be made using length measurements. However, there is no full agreement on the definition of nanostructures. Thus, nanostructures can be defined, in a narrow context, as structures with at least two dimensions below 100 nm [3, 5] or, in a broad approach, as structures with one dimension below 100 nm and a second one below 1 μm [1, 6].

Currently, one of the compounds of interest in micro/nanoscience, that was subjected to recent research [7-12], is calcium carbonate ($CaCO_3$). It is the main constituent of limestone, marble and chalk [13] and has a broad set of potential applications in areas as diverse as biomedicine and in the paper industry [14, 15]. Thus, this compound drew the attention of researchers and will be the object of study along this thesis, which will focus on the continuous production of nanoparticles and microparticles of calcium carbonate using the NETmix technology.

1.1 Motivation and Relevance

Besides the scientific and general interest in technology, strong economic forces urged the entry into the nanoworld [1]. Since the discovery that new and improved physical properties of matter emerge at an intermediate level between atomic/molecular and bulk, materials with improved properties such as strength, electrical and thermal conductivity, optical response or elasticity have been available in the market [16].

Calcium carbonate, like other compounds, can exhibit different properties depending on the size of its constituting particles, its morphology and structure. Therefore, different polymorphs of different sizes can be more or less relevant to distinct applications. In that sense, the

understanding of the effect of process variables (as temperature, pH medium, reactants' concentration, flow rate and mixture level) is essential in the synthesis of $CaCO_3$.

1.2 Thesis' Objectives and Outline

This work aims the production of nanoparticles and microparticles of calcium carbonate using the NETmix technology.

It should be noted that the first experiments were performed in a semi-batch reactor with proper stirring and, only after the optimization of this process, was the NETmix reactor used (more detail on this type of reactor is given in Chapter 2).

The products obtained by both processes, in the semi-batch reactor and in the NETmix reactor (continuous process), were characterized using techniques such as laser diffraction for the particles' size distribution, electrophoresis and laser Doppler velocity for measurement of the zeta potential, scanning electron microscopy (SEM) to obtain the particles' images and energy dispersive spectroscopy (EDS) for elemental characterization of the samples.

The outline of this thesis is as follows.

Chapter 2 shows a literary review and mainly explores the state of the art of calcium carbonate. Initially, a brief explanation on why the properties of nanoparticles and microparticles may vary is made. Section 2.1 presents some aspects related with calcium carbonate, including its main applications (Subsection 2.1.1), its polymorphs (Subsection 2.1.2) and the various routes for its synthesis (Subsection 2.1.3). In Section 2.2, a brief explanation on the NETmix technology and its inherent advantages is given.

In Chapter 3, it is first presented a description of the materials used in the experiments (Section 3.1). Then, the experimental set-ups used are described (Section 3.2) and the rationale behind the amount of dispersant used to stabilize the product is explained (Section 3.3). The last section of this chapter (Section 3.4) identifies the instruments used in the products' characterization and briefly describes how the samples preparation was made.

Chapter 4 contains the main results of the experiments performed. This chapter is divided into two subchapters: one for the experiments performed in the semi-batch set-up (Section 4.1) and other for the continuous production experiments using the NETmix reactor (Section 4.2).

An economic analysis, using the Aspen Plus and the Aspen Process Economic Analyzer (APEA) software's, was performed and it is described in Chapter 5.

The main conclusions taken from the development of this project are summarized in Chapter 6 and, in Chapter 7, an evaluation of the work performed during this thesis (including the achieved objectives, limitations of the project and future work to be developed) is given.

2 Context and State of the Art

Properties of materials (such as strength, electrical and thermal conductivity, optical response or elasticity) can change depending on the size of its constituent particles. So, when the dimensions of the particles constituting of a material are reduced from a larger to a smaller size, its properties remain the same at first, followed by small changes, until finally, when the size drops below 100 nm, drastic changes in properties may occur [3]. In that sense, it can be said that, usually, micrometric-scale materials exhibit the same physical properties as those in the bulk form [6], while nanometric-scale materials often display a structure and a set of properties that can diverge meaningfully from those of atoms and molecules as well as those of bulk material [2]. This intermediate behaviour between molecules and bulk may provide unique properties to materials and has drawn the attention of researchers and scientists into the nanoworld [1, 6, 16].

It is known that the properties of materials can vary from the surface to the bulk. Thus, the previously mentioned behaviour can be understood, in a simplistic approach, by the comparison of the number of atoms and molecules on the surface to those in the bulk. In larger materials, the classical case, the number of atoms and molecules in the surface is smaller when compared with the number of particles in the bulk and, therefore, the properties of the material will closely relate with those from the bulk. However, when at the nanoscale this ratio is inverted and the properties of such materials are more closely associated to the states of individual molecules and of molecules on surfaces or interfaces than to the properties of the bulk material [1].

Furthermore, it can be said that microparticles follow physical principles, i.e. the laws of classical physics which rule bulk materials [1], while nanoparticles follow quantum mechanical rules [16]. This phenomenon can be explained by the principle of the particle-wave duality, introduced in 1924 by de Broglie. The mentioned principle is a crucial aspect of quantum mechanics which states that any particle can be associated with a matter wave whose wavelength is inversely proportional to the particle's linear momentum [17]. Thus, it can be said that when the size of a physical system is in the same order of magnitude as the associated wavelength of the particles that interact with the system, the behaviour of the particle is well described by the rules of quantum mechanics. For example, a macroscopic object has an associated wavelength much smaller than the object's size and, therefore, the laws of classical mechanics are applied. On the other hand, in the case of electrons orbiting around a nucleus, their associated wavelength is in the same order of magnitude as the electron-nucleus distance in a way that the use of quantum mechanics is necessary [16].

Since this thesis aims the production of nanoparticles and microparticles of calcium carbonate, a broad description of this product is presented next.

2.1 Calcium Carbonate

Calcium carbonate is the main constituent of limestone, marble and chalk [13]. It is a natural occurring and abundant mineral that represents about 4 % of the earth's crust [18, 19] and embodies the protective shells, skeletons and teeth of some living organisms [8]. For example, coral reef and shellfish produce natural calcium carbonate by incorporating mineral components and carbon dioxide (CO_2), a phenomenon known as biomineralization [20]. This mineral provides a major contribution in the sequestration of carbon dioxide [21] and negatively affects industrial water treatment due to the formation of scale from the dissolved calcium ions and CO_2 in the water [22].

The compound's global demand is driven by: the replacement of kaolin in the paper industry, the use of nano-calcium carbonate in the plastic and rubber sectors, its application as drug templates, the growing focus on increasing mineral loadings in paper and the consumption associated with the paint industry. Global production is expected to reach 98.7 million metric tons by 2020 and key players in the market include Omya AG, Minerals Technology Inc., Huber Engineered Materials, Okutama Kogyo Co. Ltd., Maruo Calcium Co. Ltd., Mississippi Lime Company and Solvay S.A [23].

Due to its wide range of applications, the capacity to control the production of $CaCO_3$ to meet certain standards (such as specific morphology, structure, particle size and purity) is of great importance [14, 18]. In the following subsections some aspects of relevance inherent to calcium carbonate, such as its applications, polymorphs and synthesis' methods, will be addressed.

2.1.1 Applications

Calcium carbonate is a known versatile filler used in composite materials such as plastics, rubbers, paper, paints, adhesives, textiles, caulks and sealants [13, 18, 24]. This compound is usually differentiated between ground calcium carbonate (GCC) and precipitated calcium carbonate (PCC). Its market by application, corresponding to the year of 2013, was distributed as shown in Figure 1.

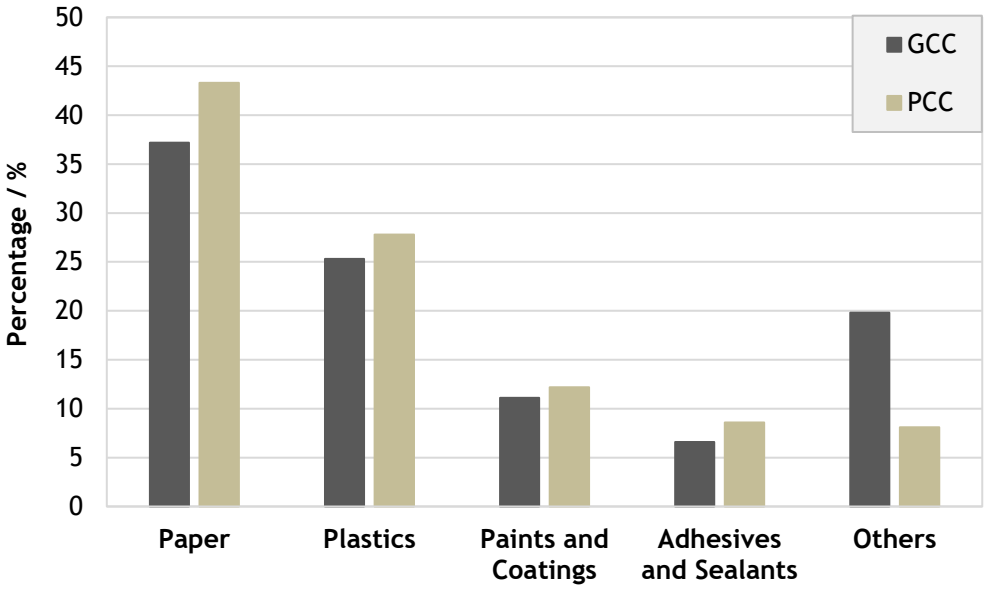

Figure 1 - End-use market structure for GCC and PCC, in 2013 [23].

In the paper industry, calcium carbonate can serve as a filler [9], since it makes the paper brighter, provides a greater resistance to yellowing and aging and it is cheaper than other alternatives, or as a part of the coatings often applied on paper. Ground calcium carbonate, with a mean particle size smaller than 1 μm, can be useful as part of coatings to improve not only the brightness, opacity, printability, ink receptivity, strength and smoothness of the paper [14], but also the rheology of coating formulations (which can be applied at coater speeds of up to 1600 $m \cdot min^{-1}$). In this specific application, the performance of ground calcium carbonate far exceeds that of the precipitated calcium carbonate [13].

Regarding the plastic industry, the use of calcium carbonate in flexible and rigid polyvinyl chloride (PVC), polyolefins (particularly polypropylene), thermosets and elastomers (including rubber) allows an improvement in mechanical properties such as modulus, heat resistance, hardness, shrinkage reduction, colour fastness, impact strength, stability, glass temperature and decomposition temperature. The use of this compound is also associated with a cost reduction, since it can be used as a bulking agent to substitute the more expensive polymers [25]. In thermosets, a greater load of calcium carbonate provides better surface characteristics [13]. The primary market for this particular filler is constituted by the polypropylene (PP) and PVC polymers [14].

Furthermore, calcium carbonate can also act as a low-cost extender for the paint and coating industries. It is used in this area with the objective of improving brightness, application properties, stability and exposure resistance [13].

Other applications include the use in non-abrasive adhesives in microelectronics and in the process of flue gas desulfurization, which consists in a set of processes that trap the sulphur-oxygen compounds produced in the combustion of coal [26].

Besides that, high purity calcium carbonate can be used in biomedical and food applications [8, 13, 15]. The referred compound fits the requirements of the food Chemicals Codex and the United States Pharmacopeia and it is listed in the U.S. Code of Federal Regulation as a food additive. Thereby, it can be used as an antacid, as a calcium supplement in foods, as a slight abrasive toothpaste, in chewing gum and in both paper and plastic for contact with food [13]. It is also applied in drug delivery, as templates for encapsulation of bioactive compounds, for encapsulation of proteins, for insoluble powder formulation in nasal drug delivery system, as bone replacement material in human periodontal osseous defects, in the construction of biosensors and for enzyme immobilization [8, 15, 27]. It has been recognized in medicine as a bone filling material due to its good osteo-conductivity, easy production and slow biodegradability [15].

Most recently, scientists have developed a new vaterite-based coating for a nanofiber material used as a scaffold to grow bone tissue cells in a shorter time [11].

2.1.2 Polymorphs

Polymorphism is the capacity of a solid material to exhibit more than one form or crystal structure. Calcium carbonate is known in the form of three anhydrous crystalline polymorphs – calcite, aragonite and vaterite [10] – or in its two hydrated forms – monohydrocalcite ($CaCO_3 \cdot H_2O$) and ikaite ($CaCO_3 \cdot 6H_2O$) [7, 28, 29]. This compound can also present itself in various amorphous forms [29]. Amorphous calcium carbonate (ACC) is a nanoparticulate, poorly ordered, metastable precursor to crystalline calcium carbonate [30].

Calcite is the most abundant polymorph and it is thermodynamically stable at ambient temperatures [13, 14, 26]. It usually presents a variety of morphologies, being the trigonal, rhombohedral, colloidal, needle-like and scalenohedral the most common [14, 18]. It is economic, nontoxic and usually used as an additive in plastics (since it helps to decrease the surface energy, opacity and surface gloss) [14]. This type of polymorph, once used as a filler, offers a better appearance and colour consistency when compared with other available fillers. It can also, in the case of the particles' size being controlled, increase the impact strength, elongation at break, notched Izod impact strength and stiffness [14].

On the other hand, aragonite is metastable under ambient temperature and high pressure [14] and irreversibly changes to calcite when heated in dry air at about 400 °C [13]. This polymorph usually displays orthorhombic, needle-like (acicular), flower-like and flake-like morphologies [14, 18]. It finds advantage in a slightly greater index of refraction than calcite

(see Table 1) and, for that reason, it is expected to have better performance properties as a filler in the paper and plastic industries [14].

Finally, vaterite is the less abundant and least stable form of calcium carbonate [14]. It is metastable to calcite and aragonite under geological conditions [13] and presents itself in an hexagonal morphology [14, 28]. This polymorph, unlike the previous ones, is not commonly produced by living organisms [19].

It should be noted that the physical and chemical properties of calcium carbonate vary depending on the composition of each polymorph [31]. Therefore, the control of the crystallization assumes a very important role in an industrial process [14, 20]. Table 1 summarizes the main differences in the properties of the calcite and aragonite polymorphs.

Table 1 - Properties of calcium carbonate polymorphs [13, 14, 26].

Property	Calcite		Aragonite (Orthorhombic)
	Rhombohedral	Scalenohedral	
Solubility product, K_{sp} / M^2	-	3.36×10^{-9}	6×10^{-9}
Solubility at 18 °C / $g\cdot g_{water}^{-1}$	1.3×10^{-5}	-	1.9×10^{-5}
Density at 20 °C / $g\cdot cm^{-3}$	-	2.71	2.93
Melting point / °C	1339 (at 10.38 MPa)	-	Decomposes to calcite at T>400 °C
Hardness (Mohs' scale)	3.0	3.0	3.5-4.0
Refractive index (RI)	1.58	1.58	1.63
Coordination number	-	6	9
TAPPI brightness	99	99	99
Surface area / $m^2\cdot g^{-1}$	6-8	9-15	9-13

Additionally, the solubility of the polymorphs increases in the opposite order of its stability, being ACC the most soluble, followed by vaterite, aragonite and calcite [28, 32]. Figure 2a shows the solubility product constant, K_{sp}, of the different calcium carbonate polymorphs as a function of temperature, T.

Furthermore, it is important to refer that, in an early stage, calcium carbonate precipitation results in ACC, which is unsteady and further transforms into calcium carbonate crystalline polymorphs in the presence of water or by heating [27, 29, 33, 34]. These resultant polymorphs are dependent on factors and conditions such as pH, temperature, supersaturation, conductivity, relative humidity and presence of impurities or additives [10, 31]. Figure 2b shows the polymorphs abundance in this early metastable stage as a function of temperature.

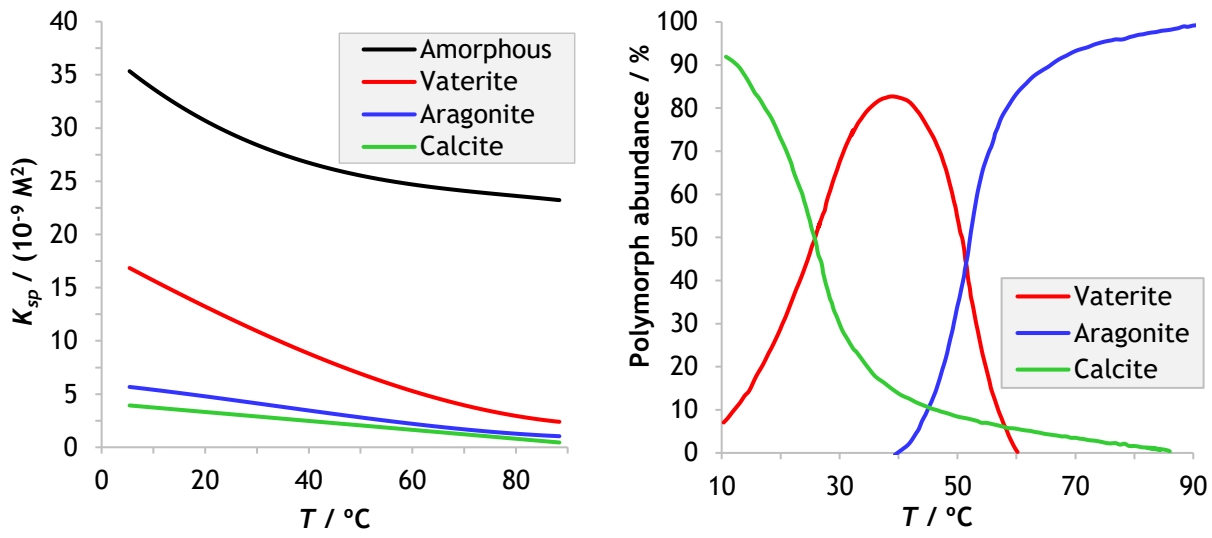

Figure 2 – Dependence with the temperature of the: (a) solubility product of calcium carbonate polymorphs and ACC [28]; (b) abundance of crystalline calcium carbonates at the early metastable stage[1] [34].

Figure 2b shows that for low temperatures (between 10 ℃ and 30 ℃) a combination of the vaterite and calcite polymorphs is formed. The vaterite polymorph is predominant from 30 ℃ to 50 ℃ and the formation of the three polymorphs occurs at temperatures between 40 ℃ and 60 ℃. Above 60 ℃, the formation of the aragonite polymorph prevails.

2.1.3 Synthesis Methods

Commercial calcium carbonate consists in two distinct types: ground calcium carbonate and synthetic/precipitated calcium carbonate.

The production of natural ground calcium carbonate begins with the quarrying (usually in an open-pit type) of naturally occurring deposits of chalk, limestone or marble. Typically, the deposits for industrial applications have a greater than 90 % $CaCO_3$ purity and high brightness. The ore is then taken into a primary crusher (for size reduction) and the following procedure is dependent on the material being produced. In that sense, two different types of processes arise: one that originates a coarse product with a purity level between 90 to 98 % and a second one that allows the production of a finer and purer material [13].

[1] for the case where precipitation was made by the rapid addition of 0.25 L of a 6.70×10^{-2} M calcium chloride solution to 0.62 L of a 1.30×10^{-2} M sodium carbonate solution and the ionic strength, I, adjusted to 0.2 M with sodium chloride.

In the first case, calcium carbonate is submitted to a secondary crushing in a crusher that may have a cone or jaw format. This process produces a smaller than 4 cm material and is usually followed by a grinding in a roller mill or ball mill, which produces products with an average particle size of 5 μm [13]. For the second mentioned case, the secondary crushing should produce a material smaller than 100 μm, allowing the mineral impurities to be separated from the ore. A flotation process, which explores the difference in hydrophobicity between compounds, is then applied to separate the impurities from calcium carbonate, resulting in a higher brightness of the material and a purity level superior to 98 %. Additionally, the product is ground in a ball mill and particles in the range of 2 to 50 μm are produced. At last, a median particle size smaller than 2 μm is obtained by the wet ground in media or sand mills. The final product is, therefore, a slurry that can be sold after the addition of stabilizers and biocides or dried into powdered product [13].

The second type of commercial calcium carbonate, PCC, can be produced by various methods. However, only the carbonation process (also known as the Kitano method [28]) is commercially used in the United States [13, 14]. This method is one of the most economically efficient, environment friendly and less energy consuming (when compared to other conventional processes) [14, 31] and consists in three main steps:

$$\mathrm{CaCO_3} \rightarrow \mathrm{CaO} + \mathrm{CO_2} \tag{2.1}$$

$$\mathrm{CaO} + \mathrm{H_2O} \rightarrow \mathrm{Ca(OH)_2} \tag{2.2}$$

$$\mathrm{Ca(OH)_2} + \mathrm{CO_2} \rightarrow \mathrm{CaCO_3}(\downarrow) + \mathrm{H_2O} \tag{2.3}$$

The first step is the calcination of limestone, usually in a kiln, between 900 ℃ and 1000 ℃ to form calcium oxide (lime) and carbon dioxide, Eq. (2.1); then, there is the treatment of the calcified lime with water, which results in milk of lime ($Ca(OH)_2$), Eq. (2.2), and the purification of the milk of lime and its subsequent reaction with carbon dioxide (obtained in the calcination step) to form calcium carbonate and water, Eq. (2.3) [13, 14]. It is important to refer that the CO_2 produced in the calcination exceeds the need of this compound in the global process [35]. This happens due to the combustion of fuel to provide heat to the endothermic calcination reaction [35].

The last step of the carbonation takes place in a reactor known as a carbonator and the end of the reaction can be monitored by, for example, pH measurements [13]. Since the solubility of calcium carbonate in water is relatively low (see Table 1), this product will precipitate. It is also important to refer that the conditions of the reaction affect the type of crystal and the size of the produced particles. Nevertheless, this traditional method is associated with the

formation of a mixture of several crystalline polymorphs with anisotropic particles. Usually, the particles are also highly agglomerated and there is inadequate control over the distribution of their sizes [25].

After the carbonation step, a screening can be performed to purify and control the maximum size of the obtained calcium carbonate. This stage is followed by a dewatering with the resource of rotary vacuum filters, pressure filters or centrifuges and the final drying of the product is achieved with a rotary, spray or flash dryer. This process results in a product with an average particle size that can vary from ca. 0.3 μm up to a few micrometres [13].

With the intent of improving the handling properties and dispersibility in plastics, some grades of calcium carbonate can be surface coated. This type of treatment includes fatty acids, resins and wetting agents and helps to reduce the surface energy and, consequently, facilitates the dispersion in organic binders [13].

Although the carbonation process is the most industrially used, the majority of research done is directed towards the method of mixing solutions containing both the carbonate and calcium ions [36] – the double salt deposition process [37]. The sources of calcium and carbonate ions greatly affect the size and morphology of the particles obtained and, usually, include salts like calcium chloride ($CaCl_2$) and calcium nitrate ($Ca(NO_3)$) and sodium carbonate (Na_2CO_3), sodium bicarbonate ($NaHCO_3$), ammonium carbonate ($(NH_4)_2CO_3$), ammonium bicarbonate (NH_4HCO_3) and potassium carbonate (K_2CO_3) [28]. This method is explored in this work, with the calcium chloride and potassium carbonate salts:

$$CaCl_2(aq) + K_2CO_3(aq) \rightarrow CaCO_3(s) + 2KCl\,(aq) \qquad (2.4)$$

When the mixing of salts is achieved under ultrasonic effects, the method is known as ultrasound cavitation technique. The ultra-sonication phenomenon provokes a uniformly disperse mixture of the reactants that will form the desired product. Simultaneously, the particles of $CaCO_3$ formed will have a tendency to agglomerate with each other due to strong electrostatic forces of attraction developed on their surfaces [12]. Afterwards, the de-agglomeration and charge nullification can be achieved by the addition of surfactants and additives under ultrasonic environment. It should be noted that the use of this type of compounds for surface modification is recurrent and has been extensively studied [12].

Furthermore, the process of mixing lime soda (calcium hydroxide) with sodium carbonate to produce sodium hydroxide and calcium carbonate is known as the lime-soda process [37].

Moreover, and with the intent of controlling the shape and size of the formed particles, the polymer mediated growth (PMG) technique emerged. In this method, one of ions is bound within

a polymer matrix and the other one is allowed to diffuse through this complex and react to form the desired compound [15].

2.2 The NETmix Reactor

This work has the main objective of continuously producing calcium carbonate particles using the NETmix technology. This reactor, internationally patented and developed at the Laboratory of Separation and Reaction Engineering (LSRE) from FEUP [38], is a static mixer that allows a high degree of both micro and macromixing quality along the reactor [39, 40]. It consists in a network of chambers interconnected by channels that create zones of complete mixing and of complete segregation, respectively [39, 41]. The network (Figure 3a) is generated by the repetition of unit cells, which consist in a chamber connected with two inlet channels and two outlet channels, oriented at 45° from the main flow direction (x axis in Figure 3a) [41]. Unit cells can be constructed from cylindrical chambers and rectangular cross section area channels, known as a 2D unit cell (Figure 3b), or from spherical chambers and cylindrical channels, the designated 3D unit cell (Figure 3c) [40].

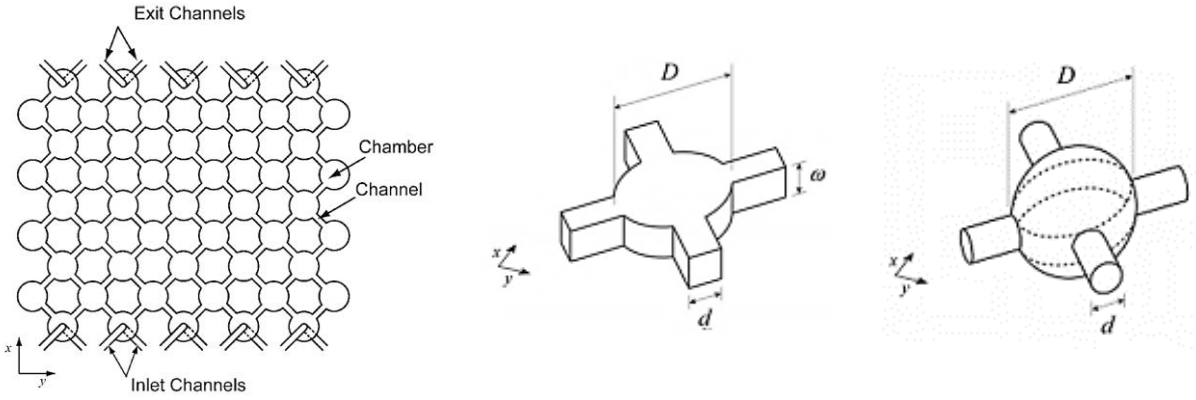

(a) (b) (c)

Figure 3 – (a) Schematic representation of the network of chambers and channels [42]; (b) 2D unit cell; (c) 3D unit cell [40].

So far, four prototypes were built: NETmix 3D, Lab-scale NETmix, Multi-Inlet NETmix and the microNETmix.

The NETmix 3D was the first prototype ever built, and 3D unit cells were used. 2D unit cells were used in the other prototypes and the transition from 3D to 2D geometries represented a significative decrease on the construction complexity [40]. Lab-scale NETmix was built for lab-scale projects with lower yields and the Multi-Inlet NETmix, which incorporates multi-inlet injection points along the reactor, is used when higher yields are required. Finally, the microNETmix reactor was idealized with the intent of lowering the reactants' demand and, consequently, shortening the time of the experiments. It also allows a higher Reynolds number,

Re, for the same flow rate and the control of the temperature due to a system of water circulation.

This last reactor was used in the experiments performed during this work. It is made of stainless steel and has 25 rows and 8 columns. It amounts to a total volume, V, of 1.3 mL, with a chamber diameter, D, of 3.3 mm and 0.5 mm of both diameter, d, and depth, ω, of the channels. Since the stoichiometry of the reaction is 1:1, Eq. (2.4), and the same molar concentration of both reactants is used, the most advantageous injection scheme and the one applied is an ABABABAB distribution, as schematized in Figure 4.

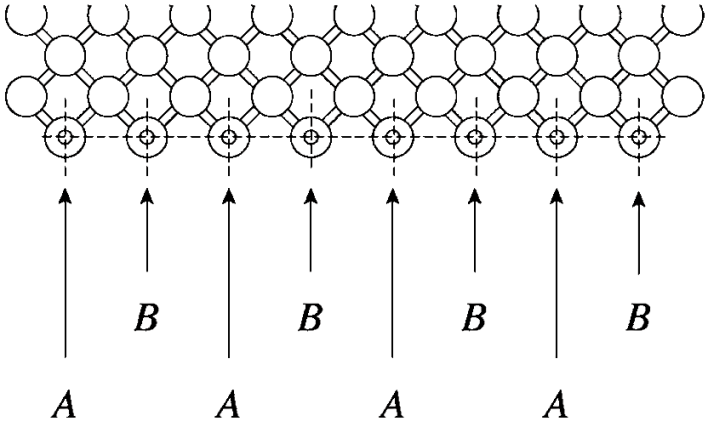

Figure 4 - Pre-mixed injection scheme [42].

The Reynolds number in the NETmix channels can be determined by:

$$\mathrm{Re}_{\mathrm{channel}} = \frac{\rho \bar{v}_{channel} d_h}{\mu} \tag{2.5}$$

where ρ is the mixture's density (kg·m^{-3}), $\bar{v}_{channel}$ the average velocity in the channels (m·s^{-1}), d_h the hydraulic diameter of the channels (m) and μ is the mixture's viscosity (Pa·s).

Through tracer experiments, it was verified, for a Reynolds range from 75 to 200, a continuous increase in the mixing dynamics, which ended up making the chamber homogenization nearly instantaneous (particularly for $\mathrm{Re} > 200$) [42]. Usually, a value of 150 is taken as critical.

Finally, it is important to highlight that advantages inherent to the NETmix technology include its simple structure, the possibility of use of various injection schemes, the control of the mean residence time of the reactants and of the mixing intensity and scale, an easy control of temperature, pressure and concentration, a large surface area which favours easy heat exchange that can be used for temperature control in both endothermic and exothermic reactions, the possibility of use of different materials for its construction and an easy scale-up (due to the fact that two or more NETmix reactors can be associated in parallel or in series) [39].

3 Materials and Methods

3.1 Materials

In the experiments performed, calcium chloride and potassium carbonate were the source of calcium and carbonate ions, respectively. The reactants used were from Labkem and had a ≥94 % purity in the case of calcium chloride and >99 % purity for potassium carbonate.

Also, the effect of the use of two dispersants was studied: sodium citrate (with 99 to 100.5 % with reference to the dried substance) was used as a hydrophilic compound and sodium oleate (with ≥82 % fatty acids basis) as a hydrophobic one. Both reactants were from Sigma-Aldrich.

It is also important to highlight that all solutions were prepared with distilled water and that, in some cases, commercial calcium carbonate was analysed as a reference. A product with assay values between 98.5 and 100.5 % from Labkem was used.

3.2 Experimental Set-up

Two different experimental set-ups were used. In an early stage, the experiments were carried out in a semi-batch reactor with a high-speed dispersing and homogenizing device (Figure 5a) and, later, the formulation developed was transferred to the microNETmix reactor (Figure 5b).

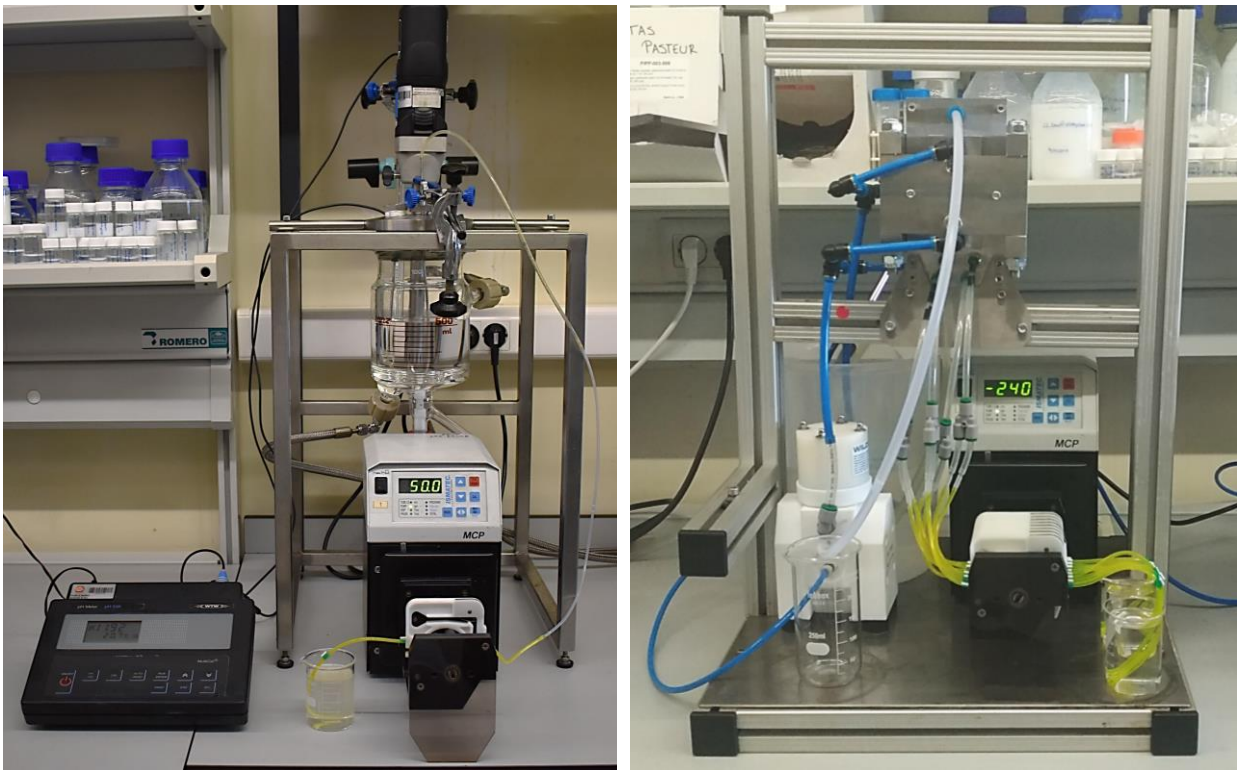

(a) (b)

Figure 5 - Experimental set-up with (a) a semi-batch reactor; (b) the NETmix reactor.

In the semi-batch set-up (Figure 5a), one reactant is placed inside the reactor's tank while the other is introduced in the system using a peristaltic pump (Ismatec MCP) and an injector (to make sure the fluid is injected directly below the dispersing device). Temperature and pH are continuously measured during the reaction and stirring is achieved by a high-speed dispersing and homogenizing device (MICCRA Homogenizer Disperser D-9) at 11 000 rpm. At the end of the reaction, both reactants were fully consumed, since the stoichiometry of the reaction is 1:1 and the number of moles of both reactants was the same.

For the NETmix experimental set-up (Figure 5b), the same peristaltic pump is used to pump the reactants solution into the NETmix and temperature control is made with the resource of a diaphragm pump (Wilden UNITEC UA).

After the precipitation of calcium carbonate, the suspension is washed and filtered. The washing step is necessary to remove the potassium chloride formed in the reaction and dissolved in the water. The product is then either dried or stored in distilled water or in a solution. Two different dispersants were investigated: a hydrophilic and a hydrophobic.

All the experiments were performed at ambient pressure. The semi-batch experiments had the main objective of evaluating the effect of the storage conditions in the stability of the product over time and the NETmix experiments were more directed towards the study of the effect of certain process variables (Reynolds number, reactants' concentration, reaction temperature and dispersant) in the final product.

3.3 Formulation: Amount of Dispersant

The effect of the addition of two distinct dispersants was studied: sodium oleate (a hydrophobic compound) and sodium citrate (a hydrophilic compound). Now, it seems intuitive that the amount of dispersant needed to stabilize the $CaCO_3$ particles is dependent on the mass of the same. It is understood that the dispersant will cover the calcium carbonate particles and, consequently, prevent the interaction between the particles and block surface reactions that provoke the recrystallization of particles and/or aggregation of the same.

In that line of thought, it is understandable that the number of molecules of dispersant that cover one crystal of calcium carbonate, $N_{disp|_{1c}}$, is given by:

$$N_{disp|_{1c}} = \frac{S_c}{TPSA_{disp}} \tag{3.1}$$

where S_c is the surface area of a calcium carbonate crystal and $TPSA_{disp}$ is the topological polar surface area (TPSA) of a molecule of dispersant. As a simplification, it was assumed a cubic shape with a length of 20 nm for the calcium carbonate crystals. The TPSAs were taken as 1.41 nm^2 to sodium citrate and 0.401 nm^2 to sodium oleate [43, 44].

Furthermore, it is assumed that the total number of molecules of dispersant to cover all calcium carbonate crystals, N_{disp}, is given by:

$$N_{disp} = n_c N_{disp|_{1c}} \alpha \tag{3.2}$$

where n_c represents the number of crystals of calcium carbonate and α is the number of layers of dispersant assumed.

On the other hand, the number of crystals can be estimated as:

$$n_c = \frac{V_{CaCO_3}}{V_c} \tag{3.3}$$

where V_{CaCO_3} is the total volume of calcium carbonate and V_c is the volume of one crystal of calcium carbonate (once again assuming cubic shape and a length of 20 nm). On this last equation, the total volume of $CaCO_3$ can be obtained by:

$$V_{CaCO_3} = \frac{m_{CaCO_3}}{\rho_{CaCO_3}} \tag{3.4}$$

where m_{CaCO_3} is the mass of calcium carbonate and ρ_{CaCO_3} its density.

Finally, making use of the Avogadro's constant, N_A, and the molecular weight of the dispersant, MW_{disp}, the mass of dispersant, m_{disp}, can be calculated as:

$$m_{disp} = \frac{N_{disp}}{N_A} MW_{disp} \tag{3.5}$$

3.4 Sample Characterization

The obtained product ($CaCO_3$) was then characterized by the techniques presented below. A more detailed description of them is presented in Appendix A.

3.4.1 Laser Diffraction for Particle Size Analysis

This type of analysis was performed by a Beckman Coulter (model LS230) apparatus that has a size range of 0.04 to 2000 μm. This equipment uses a laser light with 750 nm wavelength to size particles from 0.4 to 2000 μm by light diffraction and polarization intensity differential scattering (PIDS) to classify particles with a size between 0.04 and 0.4 μm and enhance the size distribution obtained by the diffraction method up until 0.8 μm [45]. It should be noted that the equipment used has three sets of polarized filters that provide polarized monochromatic light at three different wavelengths: 450 nm (blue), 600 nm (orange) and 900 nm (near-infrared, invisible) and, thus, allows three independent measurements of the PIDS effect [45].

It is important to refer that an optical model appropriated for calcium carbonate particles was used. The parameters considered in the same are listed in Table 2.

Table 2 - Properties of the optical model used [45].

Fluid RI (Real)	1.333
Sample RI (Real)	1.480
Sample RI (Imaginary)	0.010

3.4.2 Electrophoresis and Laser Doppler Velocimetry (LDV)

The apparatus used was the Malvern ZetaSizer Nano ZS equipment (with a 632.8 nm "red" laser), that is limited, for this type of measurement, from 5 nm to 10 μm. The product to analyse was diluted in distilled water and, therefore, the predefined values of the ZetaSizer software for water ($T = 25\,℃$, $RI = 1.330$, $\mu = 0.8872\,\mathrm{cP}$ and $\varepsilon_r = 78.5$) were used. As the material to analyse was calcium carbonate, an RI of 1.630 and an absorption value of 0.010 were defined.

3.4.3 Scanning Electron Microscopy (SEM) and Energy Dispersive Spectroscopy (EDS)

Both analyses were performed with a Phenom ProX G4 equipment and sample preparation included the pouring of a few drops of solution into a carbon tape (which was glued to a metallic support). After the evaporation of the solvent (at ambient temperature), the samples were passed through compressed air and analysed.

3.4.4 Nitrogen Adsorption

Brunauer-Emmett-Taylor (BET) surface area measurements were performed in the Laboratory of Catalysis and Materials (LCM) in a high-speed surface area and pore size analyser from NOVA series (4200e). The software used was the Quantachrome NovaWin (data acquisition and reduction for NOVA instruments).

3.4.5 Fourier-Transform Infrared Spectroscopy (FTIR)

For this analysis a Bomem arid zone MB series spectrometer, in a wavenumber range from 500 to 2000 cm^{-1}, was used. Sample preparation consisted in the formation of a pellet containing powder of potassium bromide (97 to 99 % w/w) and of the product to analyse.

3.4.6 Transmission Electron Microscopy (TEM)

This type of analysis was performed at the International Iberian Nanotechnology Laboratory (INL) in a JEOL JEM 2100 microscope with an acceleration voltage of 200 kV. Sample preparation included the dispersion of calcium carbonate powder in water by means of ultrasounds and its subsequent spreading into a TEM grid (Ted Pella - #01824) made of ultrathin carbon film on a lacey carbon support film.

4 Results and Discussion

As previously stated, the experiments were performed in two distinct set-ups. On one hand, the semi-batch experiments had the primary objective of studying the effect of the storage conditions on the stability of the produced calcium carbonate particles. For the purpose, the product was stored under different solutions and temperatures and it was analysed over time. On the other hand, in the NETmix experimental set-up it was intended to study the influence of several process variables (such as the Reynolds number, temperature, type and amount of dispersant and reactants' concentration) in the final product.

The results to both types of experiments are presented below.

4.1 Semi-batch Experiments

Table 3 lists the experiments performed in the semi-batch set-up as well as the product's storage conditions.

Table 3 – List of experiments performed in the semi-batch set-up.

Experiment		C_{CaCl_2} / M	$C_{K_2CO_3}$ / M	Storage solution	Storage temperature / ℃
B1	a	4.0	0.8	Water	20
	b			Sodium oleate (one layer)	
	c			Sodium citrate (one layer)	
B2	a	4.0	0.8	Water	7
	b			Sodium oleate (one layer)	
	c			Sodium citrate (one layer)	
	d			Sodium citrate (two layers)	

In both batches, the reaction was completed under the same conditions (ambient temperature and pressure) and the final product was divided into three (experiment B1) or four (experiment B2) equal shares. Posteriorly, the product was filtered and stored into distinct solutions and under different temperatures so that the effect of the storage conditions in the particles' stability could be studied over time.

It should be noted that, in this type of experiments, the dispersants were only added as part of the storage solutions and were not present during the reaction. The precipitation of calcium carbonate was also made in the presence of dispersants and no significative changes in the final product were observed, being, therefore, concluded that the presence of these compounds during the reaction was not necessary.

4.1.1 Scanning Electron Microscopy (SEM)

Analysis of SEM images allowed the visualization of the shape and size of the produced particles and how these changed over time. They are presented, for the product of experiments B1 and B2 over time and for the three storage solutions tested (distilled water, sodium oleate solution and sodium citrate solution) in Figure 6, Figure 7 and Figure 8, respectively.

It should be noted that the product of experiment B1 was stored under ambient temperature, that is, approximately 20 ℃ and the product of experiment B2 was stored in a fridge at about 7 ℃.

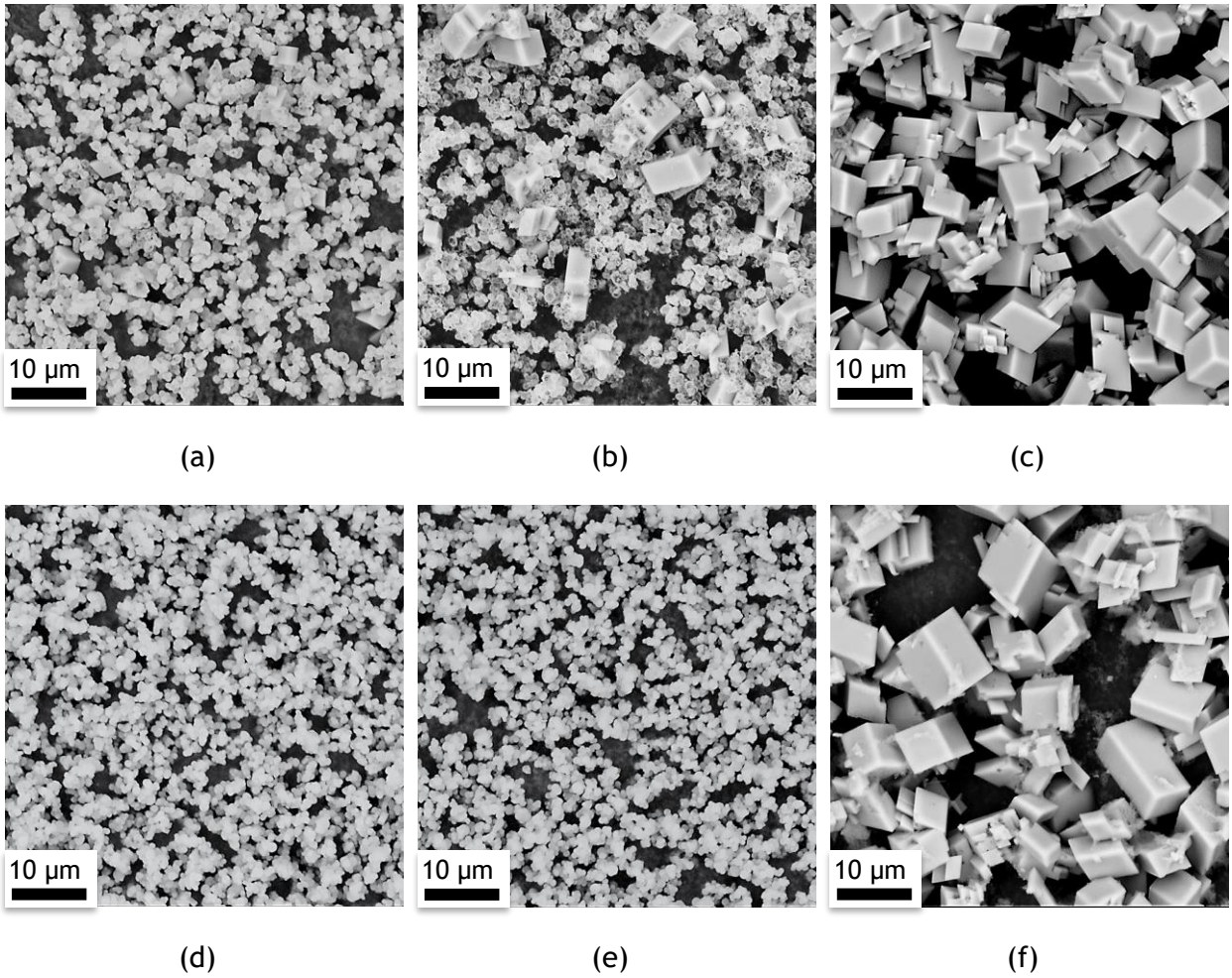

Figure 6 - SEM images of sample B1a for (a) 0 hours, (b) 48 hours and (c) one week and of sample B2a for (d) 0 hours, (e) 48 hours and (f) one week.

From Figure 6, it is observable that when the particles were stored in distilled water, recrystallization started to occur, for experiment B1, at 48 hours (Figure 6b) and, by week one, all the smaller particles had turned into larger ones of rhombohedral morphology (Figure 6c). Now, all this happened to a storage temperature of 20 ℃ (experiment B1). When a lower temperature was used (experiment B2), it was expected that this effect would be delayed. From Figure 6f it can be seen that, once again, a full recrystallization of the particles happened

by the end of one week. Nevertheless, comparing Figure 6b and Figure 6e, the effect of the storage temperature is clear: lower temperatures slow down surface reactions and the consequent recrystallization of the particles, allowing the stability of the product for a longer period of time. It is also concludable (from the comparison of Figure 6c and Figure 6f) that temperature had no effect in the shape to which calcium carbonate recrystallized.

In an attempt to prevent the recrystallization of the particles over time and, therefore, improve their stability, surface modification by means of the use of two distinct dispersants was studied. Sodium oleate, an hydrophobic compound, and sodium citrate, an hydrophilic compound, were tested. The results are shown in Figure 7 and Figure 8.

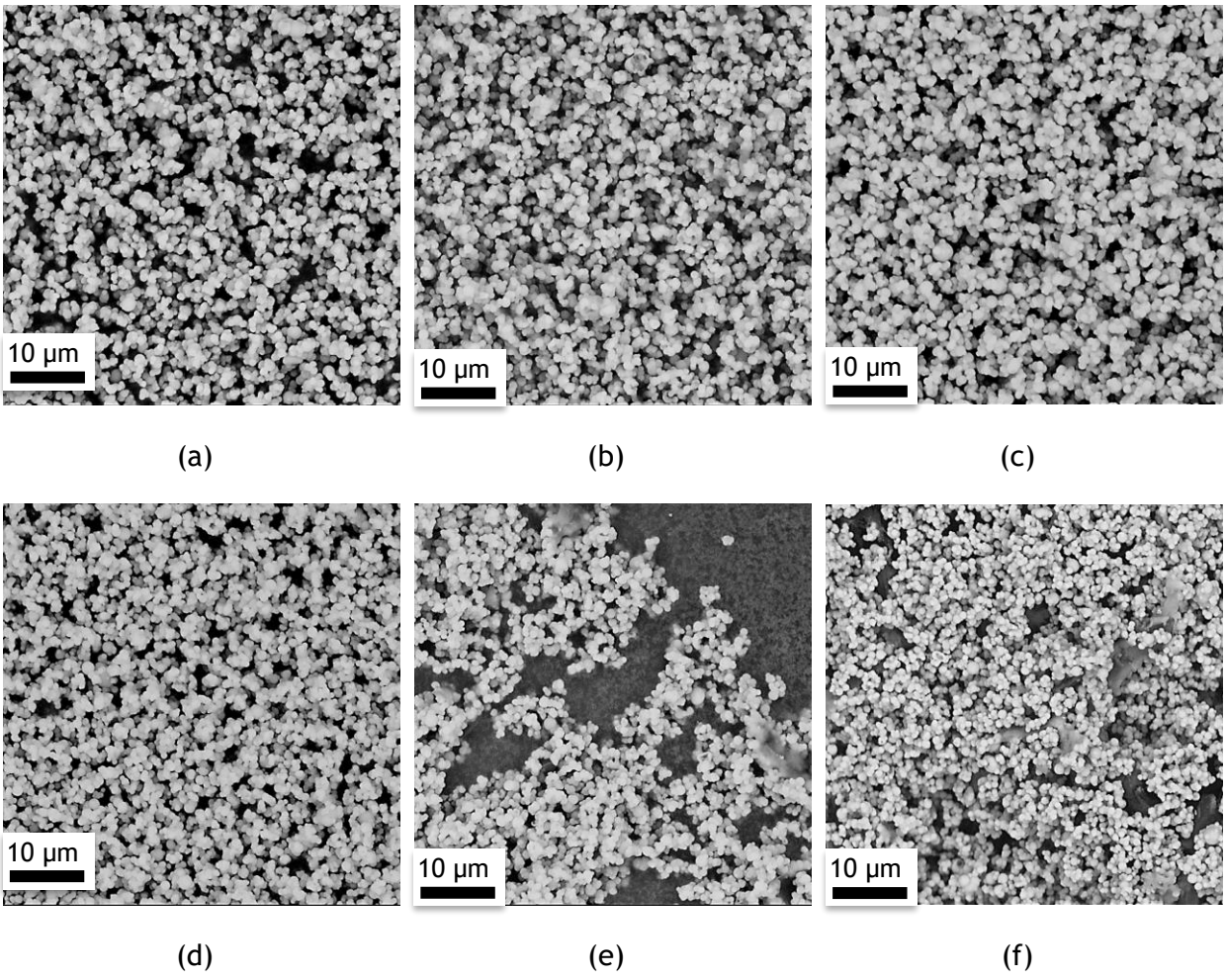

Figure 7 - SEM images of sample B1b for (a) 0 hours, (b) 6 weeks and (c) 16 weeks and of sample B2b for (d) 0 hours, (e) 6 weeks and (f) 16 weeks.

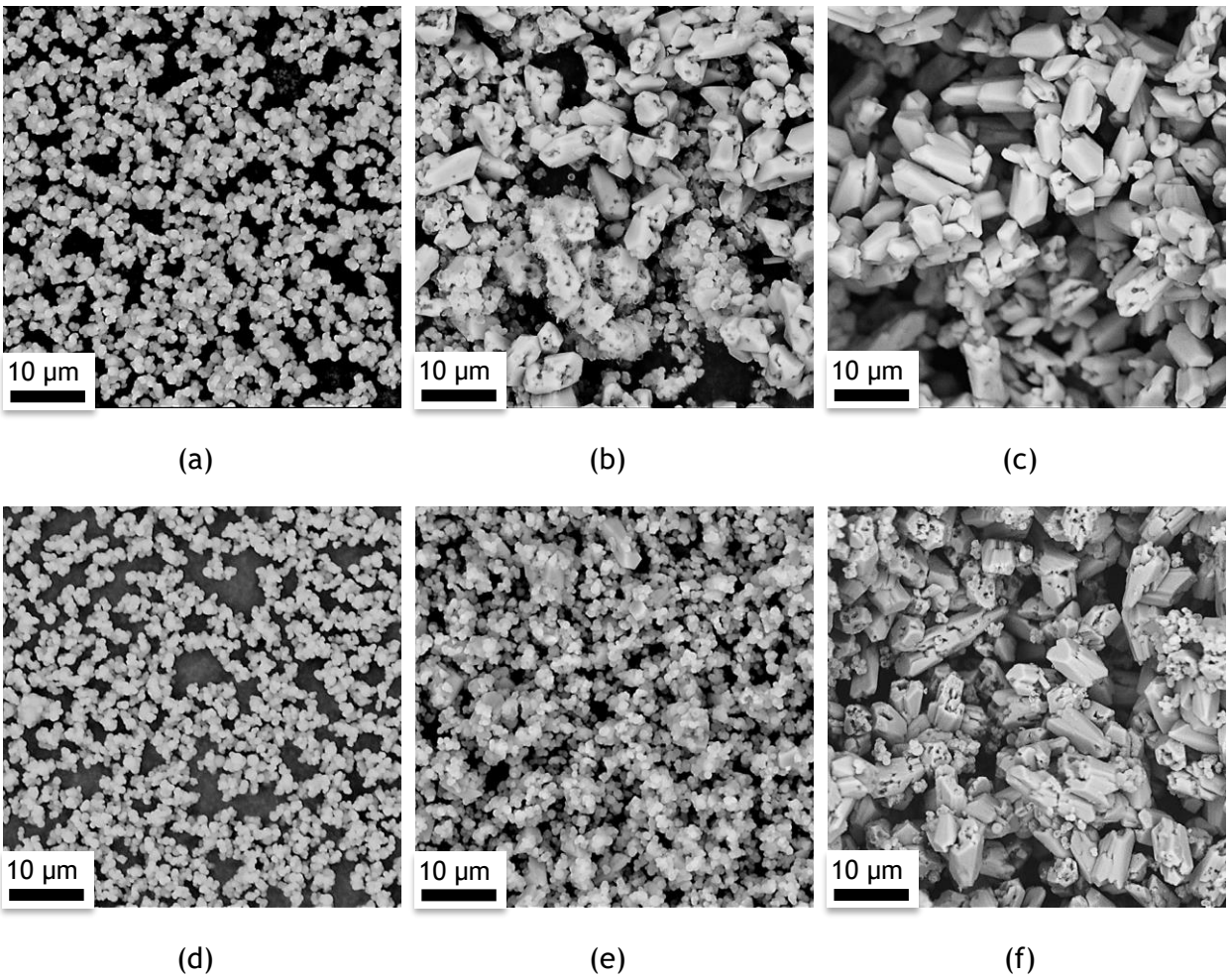

Figure 8 - SEM images of sample B1c for (a) 0 hours, (b) 3 weeks and (c) 16 weeks and of sample B2c for (d) 0 hours, (e) 3 weeks and (f) 16 weeks.

Comparing Figure 7 and Figure 8, it can be easily concluded that the inhibitory effect of sodium oleate on the surface reactions that cause the recrystallization of the particles is greater than that of sodium citrate. Nevertheless, both dispersants had a positive outcome.

For experiment B1 and the case where a storage solution of sodium oleate was used, it was verifiable that, even after 16 weeks (Figure 7c), the particles remained of the same morphology (size and shape) as in time zero (Figure 7a). This was also verifiable in the case where the storage temperature was about 7 ℃ (Figure 7f). This result was expected since it was seen that higher storage temperatures are favourable to the occurrence of the surface reactions that lead to the recrystallization of the particles. If it was proved that at 20 ℃ (experiment B1), 16 weeks were not enough time to affect the product's stability, the same amount of time should not be sufficient for the particles to recrystallize at a lower temperature (experiment B2).

On the other hand, in experiment B1 and when the product was stored in a sodium citrate solution, it was clearly evident, by week 3 (Figure 8b), the recrystallization the particles (although smaller particles were still visible) and, by week 16 (Figure 8c), it was seen that the

product had fully recrystallized. Furthermore, it should be highlighted that the storage in a solution of sodium citrate affected the shape to which the calcium carbonate particles recrystallized. Moreover, and despite the fact that it was opted not to show that image, it was seen that, in week 1, the particles still had not started to recrystallize, which proves a clear improvement of the particles' stability upon the addition of sodium citrate and when compared with the case B1a (where they were stored in distilled water).

Comparing SEM images of experiments B1 and B2, it was conclusive that the level of recrystallization for particles of the same age was evidently smaller in the case where the storage temperature was 7 ℃. Comparing Figure 8b with Figure 8e and Figure 8c with Figure 8f this effect is clearly noticeable. Furthermore, in Figure 8f, as opposed to Figure 8c, it was still visible that the particles had not fully recrystallized, which is another strong evidence of the effect of the storage temperature.

Finally, and as in both the experiments B1c and B2c it was proven that a storage solution containing the equivalent to one layer of sodium citrate was not enough to prevent the recrystallization of the product within 16 weeks, the effect of a storage solution with twice as much dispersant was studied for a storage temperature of about 7 ℃ (Figure 9).

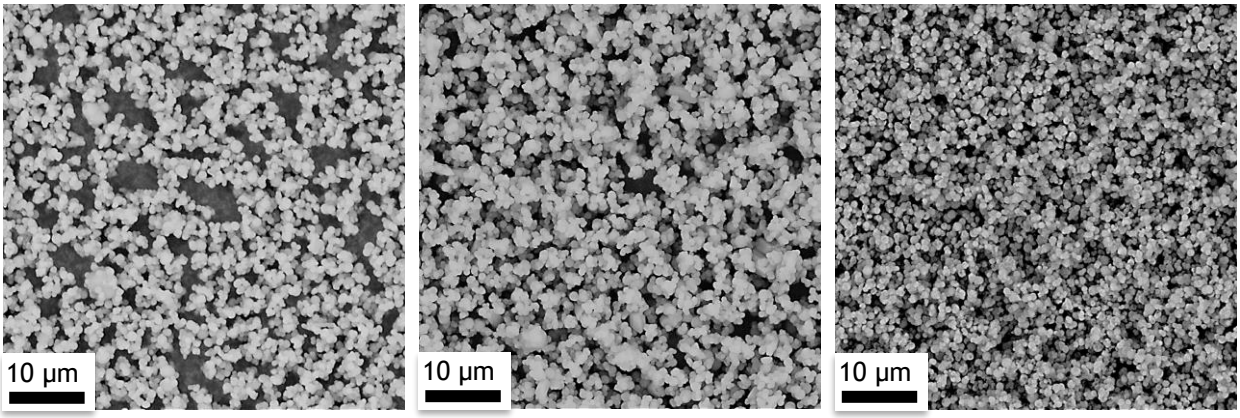

(a) (b) (c)

Figure 9 - SEM images of sample B2d for (a) 0 hours, (b) 3 weeks and (c) 16 weeks.

Upon closer inspection of Figure 9b (for 3 weeks), it is possible to observe the formation of very few straight boundary particles, indicatory of the start of recrystallization. However, this characteristic did not seem to aggravate in time (Figure 9c). Hence, it was conclusive that an increase of the concentration of sodium citrate was favourable to the stability of the product, as expected.

From the observation of the previous figures, it can be said that, in the initial instant (Figure 6a, Figure 6d, Figure 7a, Figure 7d, Figure 8a, Figure 8d and Figure 9a), small spherical particles of calcium carbonate in the order of one micron are formed. As no significative difference

between the particles formed in experiment B1 and B2 is observable for time zero, it is understood that the experience is repeatable.

4.1.2 Transmission Electron Microscopy (TEM)

SEM analysis of the calcium carbonate on its production day showed what appeared to be spherical particles of approximately 1 μm. However, when the samples were taken to a higher resolution microscope – the transmission electron microscope (TEM) – the obtained images differed significantly and allowed a better understanding of the morphology of the produced particles.

Figure 10 presents a set of TEM images of the calcium carbonate produced in the semi-batch experiment for different ampliations. It is important to mention that this product was dried at ambient temperature and that no dispersant was added.

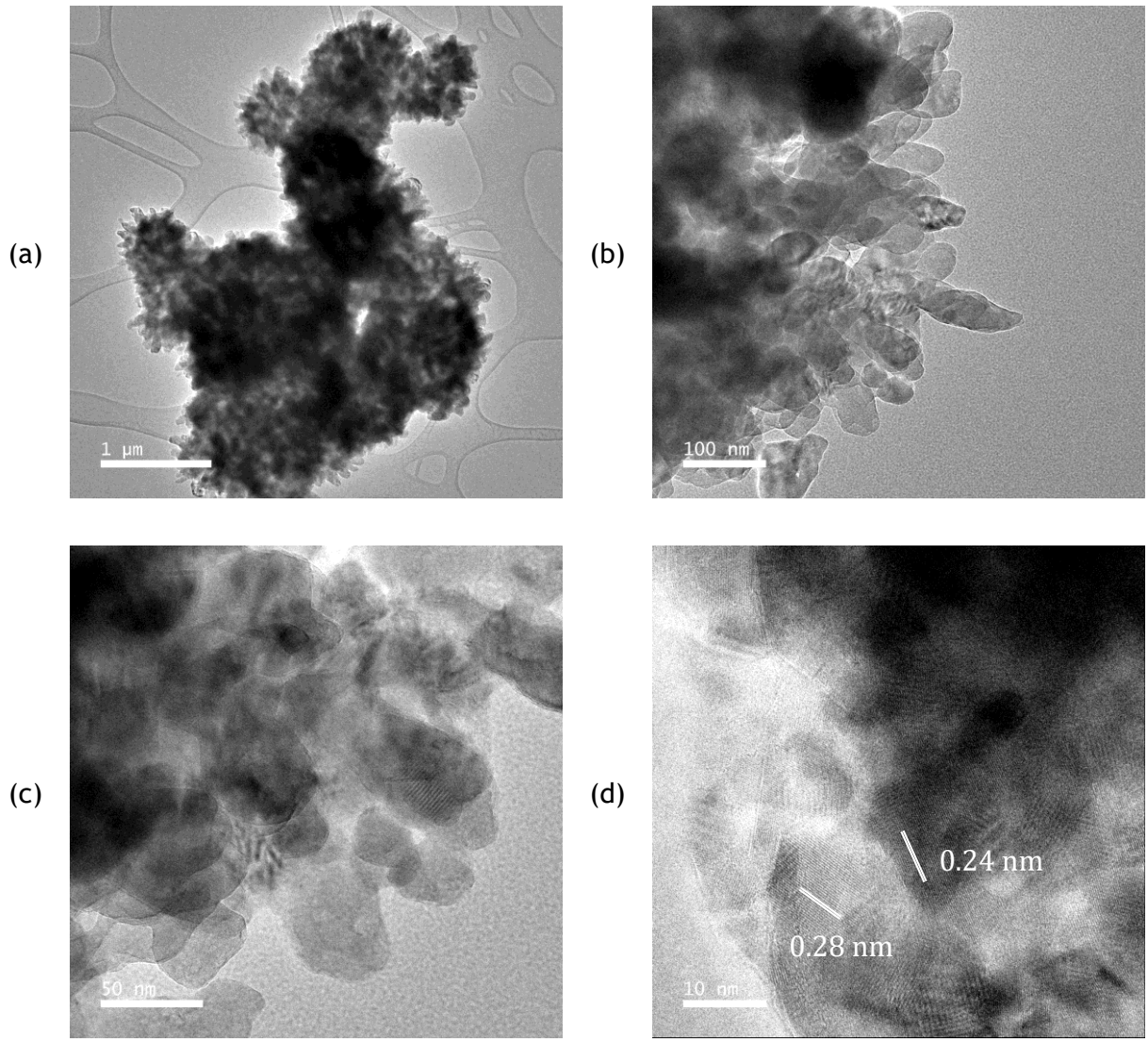

Figure 10 - TEM images of the calcium carbonate on its day of production with an ampliation of (a) 10k, (b) 80k, (c) 200k and (d) 800k times.

From Figure 10, it is possible to conclude that what appeared to be spherical particles of approximately 1 μm are indeed highly agglomerated nanoparticles of calcium carbonate. Even though sample preparation included an ultrasound treatment, it is still visible, from Figure 10, that this was not enough to separate the particles and, therefore, a proper morphological characterization of size and shape of the particles was not conceivable. Despite that, from the observation of Figure 10b and Figure 10c, it is possible to infer that nanometric particles (of size smaller than 100 nm) are formed.

Furthermore, in Figure 10d, patterns indicating crystalline structures are clearly visible. This quickly excludes the hypothesis that amorphous calcium carbonate is being produced. Moreover, and by observing and measuring diffraction patterns (DPs), it is possible to distinguish between the different crystal structures of calcium carbonate: calcite, vaterite or aragonite.

Appendix B contains information about the fringe spacings, δ, and the angle between them, 2θ, for different crystallographic directions and for the three calcium carbonate phases. Comparing the data shown in Figure 10d with the one in Appendix B, it is possible to conclude that a fringe spacing of 0.24 nm matches with aragonite δ_{200} and δ_{031} and with calcite δ_{110}. Furthermore, a fringe spacing of 0.28 nm can correspond to aragonite δ_{002} or calcite δ_{006}. No matching with the vaterite phase was found.

Other images of this analysis are presented in Appendix B, however, none of them allowed the univocal identification of the calcium carbonate phase. For that, two fringe spacings in the same region of the sample and the angle between them would be necessary. Since this was not possible to obtain, an alternative approach for phase identification would be x-ray diffraction (XRD).

4.1.3 Energy Dispersive Spectroscopy (EDS)

Following each experiment, an EDS analysis was performed. Figure 11 and Figure 12 show the tested regions and corresponding EDS spectrums for the experiments B1 and B2, respectively.

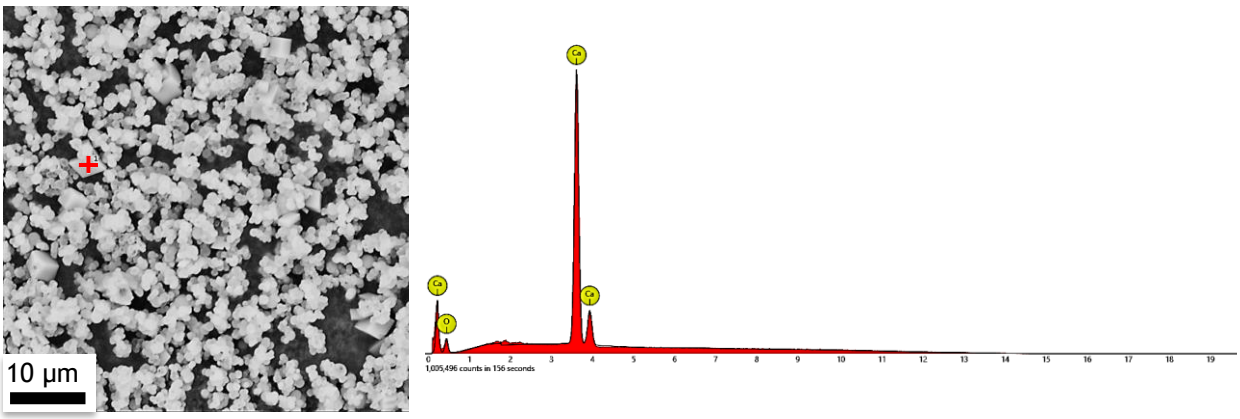

(a) (b)

Figure 11 – (a) Tested region and (b) respective EDS spectrum for sample B1.

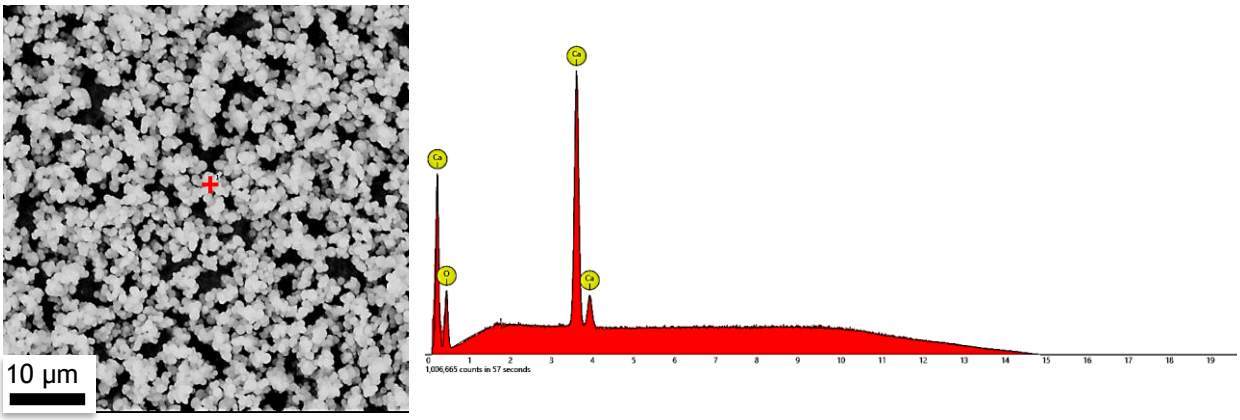

(a) (b)

Figure 12 – (a) Tested region and (b) respective EDS spectrum for sample B2.

As it can be expected, calcium and oxygen were detected in both analysis. It was also verified the absence of chloride and potassium ions, which means that the washing in the filtration step was sufficient to remove all the potassium chloride formed during the reaction.

4.1.4 Particle Size Distribution

The particles' size distribution was measured on the day of the production of the particles and in the following weeks. Figure 13 shows the volumetric size distribution of the particles of experiment B2 over time for the different storage conditions studied. It should be noted that the following measurements were obtained through the laser diffraction and PIDS techniques.

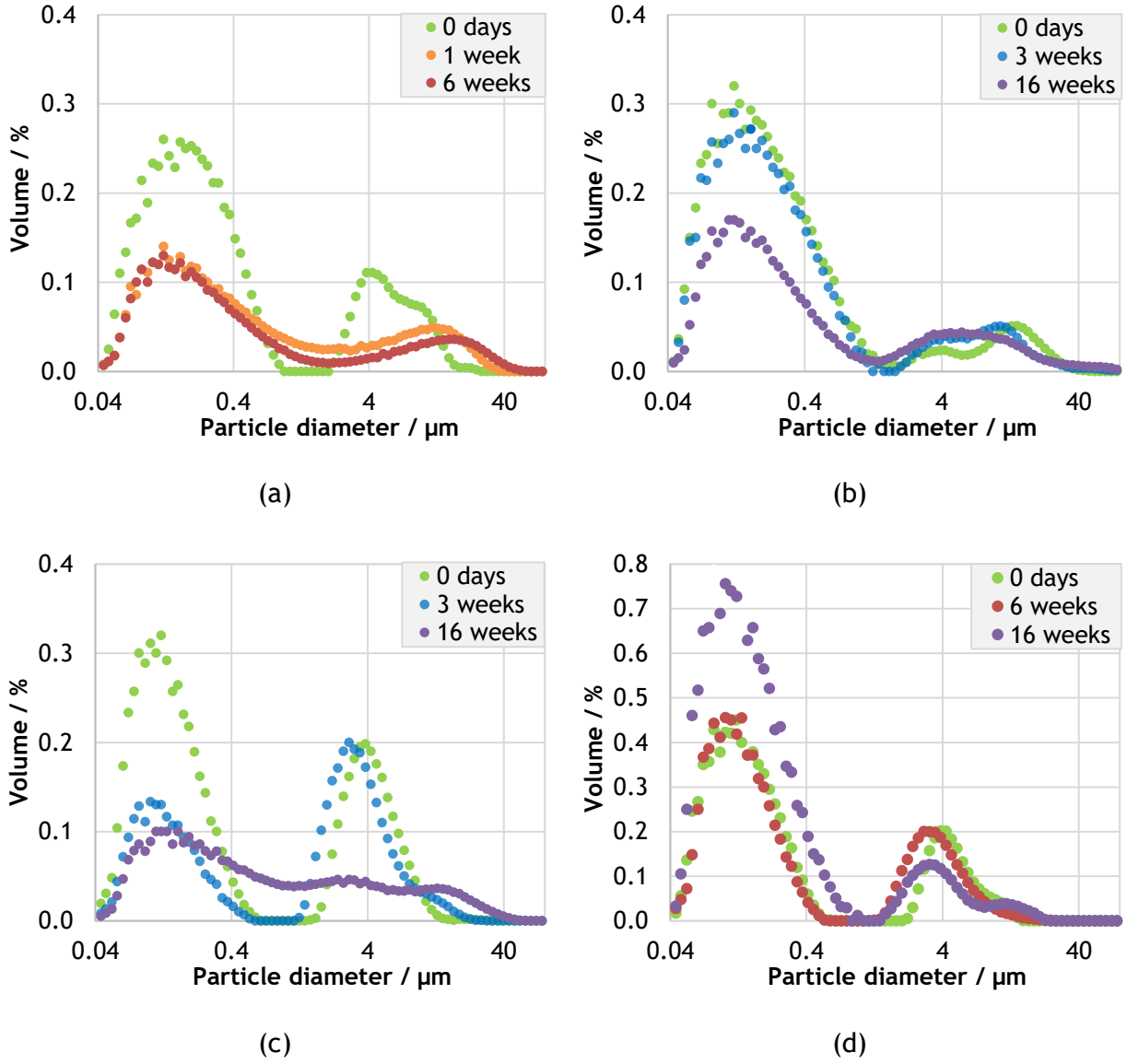

Figure 13 - Particles' size distribution over time for sample B2. Sample stored in (a) distilled water, (b) sodium oleate solution, (c) one-layer solution of sodium citrate and (d) two-layer solution of sodium citrate.

Before the examination of Figure 13, it is important to highlight that the analysis of the results here presented can lead to false conclusions and it is subjected to interpretation. Per example, if the particles are aggregated, then the size of the aggregates will be measured instead of the individual particles. Since both SEM and TEM images showed a great tendency for the calcium carbonate particles to aggregate, this aspect must be weighed carefully when analysing the size distribution curves.

Figure 13a shows the size distribution over time for the particles of experiment B2 that were stored inside distilled water. The curve from day zero shows a bimodal distribution, being that the first peak indicates the presence of particles whose diameter size is between 0.04 and 1 µm. This result is, therefore, compatible with the particle size seen on the SEM and TEM

images. On the other hand, the second peak is referent to larger sizes and most likely results from the reading of clusters and not individual particles. The curves corresponding to weeks 1 and 6 are nearly coincident and detect larger particles than those present on the day zero. A clear decrease in the intensity of the first peak is visible and the second peak is displaced to the right, indicating the presence of larger particles. This was expected since it was verified that, by the end of week 1, all particles had already recrystallized into larger ones.

The curves for the size distribution of the particles of experiment B2b (stored in a solution of sodium oleate at about 7 ℃) over time are presented in Figure 13b. SEM analysis had proven the stability of the particles during, at least, 16 weeks and, for that reason, it was expected that all curves were to be coincident. Despite small differences, this was verified for day zero and week 3. However, the size distribution curve for week 16, although similar to those of day zero and week 3, presented a clear decrease in the intensity of the first peak. The tendency for the particles to agglomerate (due to a not so good homogenization of the sample before the analysis, for example) is a possible justification for the occurrence.

Figure 13c shows the size distribution curves for experiment B2c (stored in a one-layer sodium citrate solution and inside a fridge). The curve corresponding to day zero presents a bimodal distribution, where the first peak has diameter sizes equivalent to the ones seen in SEM images and the second peak likely results from the reading of aggregates. By week 3, it was seen, in SEM images, that very few particles of calcium carbonate had already recrystallized. The diminish in intensity of the first peak of the size distribution curve can, therefore, be explained by the fact that smaller particles are aggregating and recrystallizing into larger ones. At last, the size distribution curve for week 16 shows the presence of particles in the range of 0.04 to 40 μm. By this time, SEM images show that the majority of the particles had already recrystallized, although the presence of some smaller particles was still visible. This fact accords with the verified curve.

Finally, Figure 13d presents the size distribution curves over time for the particles of experiment B2 that were stored in a two-layer solution of sodium citrate. Since SEM images showed that these storage conditions did not provoke a pronounced recrystallization of the particles for, at least, 16 weeks, it was expected that all curves were to be coincident. Despite small differences, this tendency is verified. It should be highlighted that the major discrepancy observed was in the intensity of the first peak of the size distribution curve for week 16.

It is important to underline that the graphs of the size distribution for the particles of experiment B1 over time are not presented here by choice, since they follow the same tendency and respect the same rationale as seen above.

4.1.5 Zeta Potential

The zeta potential value, ζ, was measured for experiment B2 over time. Table 4 summarizes the mean measured values for the different storage solutions tested (a, b, c and d).

Table 4 - Zeta potential mean values over time for the calcium carbonate particles of experiment B2 and the different storage solutions.

	ζ / mV			
	1 week	**3 weeks**	**6 weeks**	**16 weeks**
a	-12.5	-33.5	-28.7	-28.9
b	-20.5	-4.9	-44.3	-28.1
c	-7.1	-10.0	-11.0	-13.1
d	-14.7	-15.6	-17.1	-18.2

From the analysis of the values of Table 4, it is possible to verify that when the particles of experiment B2 were stored in distilled water, they were not stable upon 1 week of their formation. However, after this time, their stability clearly improved (the mean zeta potential value increased from -13 mV to about -30 mV). Since recrystallization was visible at week 1, and for recrystallization to occur the particles would have to aggregate, this result was expected. It was also predictable that the zeta potential absolute value after one week were to remain constant, as the recrystallization was over and the new type of particles formed should have no tendency to aggregate. This was indeed verified.

For the case B2b (storage solution of sodium oleate) no recrystallization was visible within 16 weeks being, therefore, expected that the zeta potential valued stayed constant over time. However, this tendency was not observable.

Lastly, in the cases B2c and B2d (where solutions of sodium citrate were used to store the product), a tendency for an increase of the absolute value of the zeta potential over time is seen. Despite having a lower absolute value of zeta potential than when a storage solution of sodium oleate is used, it is verifiable that an increase of sodium citrate provokes an increase of the zeta potential absolute value. Since it was verified (in the SEM images) that the addition of a higher quantity of sodium citrate allowed the stability of the product for a longer period of time, this result was expected.

4.1.6 Specific Surface Area

BET method allowed the obtainment of the specific surface area of the calcium carbonate particles. A degassing temperature of 120 ℃ for 3 hours was tested and the nitrogen adsorption and desorption isotherm obtained is shown in Figure 14. The isotherm is presented as the

adsorbed volume of nitrogen, V^a, as function of the pressure, P, normalized by the maximum pressure used, P_0.

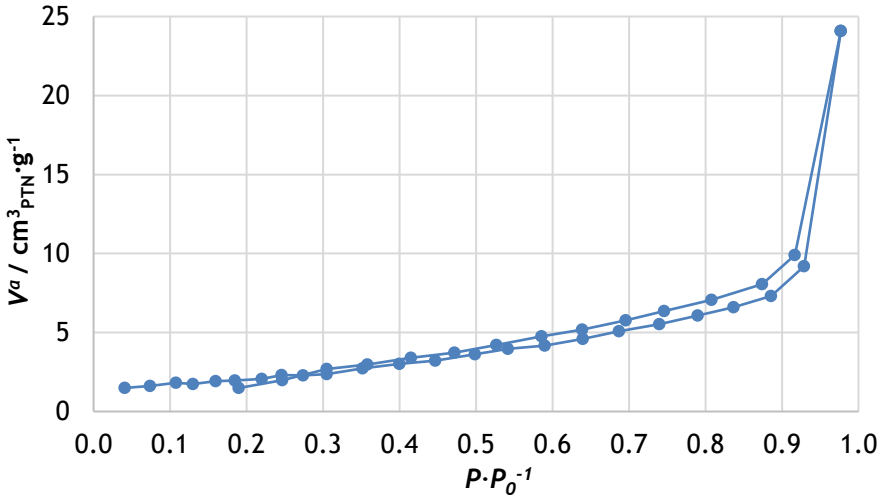

Figure 14 - Nitrogen adsorption and desorption isotherm for the product of the batch experiment.

The isotherm, shown in Figure 14, is typical of a non-porous or macro-porous material with confined multilayer adsorption and the hysteresis is characteristic of clusters (loose agglomerates) of particles with the structure of platelets (forming slit-like pores). The tendency for the particles to aggregate was clearly visible in the TEM analysis.

The BET surface area, S_{BET}, as well as the equivalent particle radius, r, is presented in Table 5. It is important to note that the radius was calculated assuming a spherical geometry and the density of calcite, 2.71 g·cm^{-3}, as indicated in Table 1.

Table 5 - BET surface area and respective radius of the calcium carbonate particles of the batch experiment.

Degassing conditions	S_{BET} / $\mathrm{m^2 \cdot g^{-1}}$	r / nm
120 °C for 3 hours	7.3	152

Since TEM images showed the presence of nanoparticles of calcium carbonate, it was expected that the radii of the particles were to be smaller than 50 nm. However, and as indicated in Table 5, this was not verified. The high tendency for the particles to aggregate could have interfered in the adsorption of the nitrogen (that only adsorbed in the outer surface of the clusters) and, therefore, resulted in an incorrect measurement of the surface area of the particles.

4.1.7 Fourier-Transform Infrared Spectroscopy (FTIR)

FTIR analysis were performed with the intent of characterizing the type of polymorph being produced. Commercial calcium carbonate and the product of the experiment B1a in the day of

its production and a week later were analysed. The resultant spectrums are presented below in Figure 15.

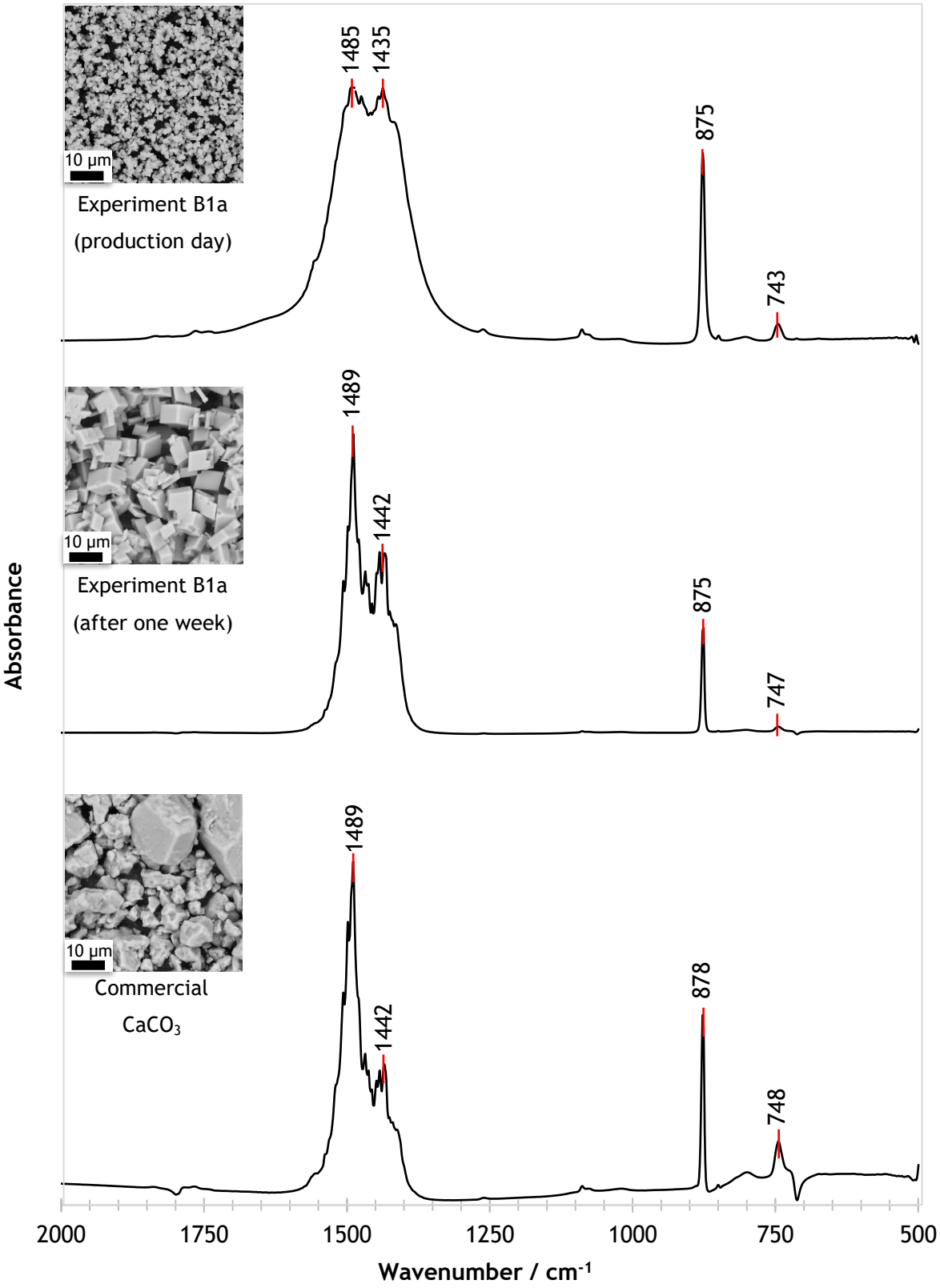

Figure 15 - FTIR spectra for both batch produced and commercial calcium carbonate.

From the comparison of the spectrums obtained and Figure 26 (Appendix A), it can be induced that the polymorph produced is vaterite. This conclusion is, however, contradictory to the more credible results obtained in TEM. Therefore, it is concluded that this type of analysis is not indicated for the identification of the polymorphs; nevertheless, since all peaks are concordant, it can be said that the same polymorph is present in all samples.

4.2 NETmix Experiments

Table 6 lists the experiments performed in the NETmix experimental set-up. In this second phase of the experiments it was intended to study the effect of variables such as the reactants' concentration, Reynolds number, reaction temperature and type and amount of dispersant on the final product.

Table 6 - List of experiments performed in the NETmix experimental set-up.

Experiment	C_{reac} / M	Re	T / ℃	Dispersant	Objective
N01	1.0	400	17	n/a	
N02	1.0	400	17	Sodium citrate (4 layers)	Study the effect of the addition of sodium citrate
N03	0.2	400	17	Sodium citrate (4 layers)	Study the effect of the reactants' concentration
N04	0.2	650	17	Sodium citrate (4 layers)	Study the effect of the Reynolds number in the reaction
N05	0.2	1500	17	Sodium citrate (4 layers)	
N06	0.2	650	17	Sodium citrate (2 layers)	Study the effect of the concentration of sodium citrate
N07	0.2	650	17	Sodium citrate (1 layers)	
N08	0.2	650	5	Sodium citrate (4 layers)	Study the effect of the temperature
N09	0.2	650	17	Sodium oleate (1 layer)	Study the effect of the addition of sodium oleate
N10	0.2	650	17	n/a	Study the effect of the reaction without dispersant
N11	0.2	650	5	n/a	Study the effect of the temperature
N12	0.2	750	17	Sodium oleate (4 layers)	Study the effect of a higher concentration of sodium oleate
N13	0.5	750	17	Sodium oleate (1 layer)	Study the effect of the reactants' concentration
N14	0.5	400	17	Sodium oleate (1 layer)	Study the effect of the Reynolds number

It should be noticed that all experiments were performed under temperature control, through a system of water circulation at approximately 17 ℃, except for experiments N08 and N11, where it was planned to study the effect of the reaction temperature and, therefore, the circulating water was at 5 ℃.

Since the focus on this part of the work was on the effect of certain variables in the final product, the stability of the particles over time was not inspected. Results are presented below.

4.2.1 Scanning Electron Microscopy

SEM images of the produced particles for each experiment are presented in Figure 16, Figure 17 and Figure 18.

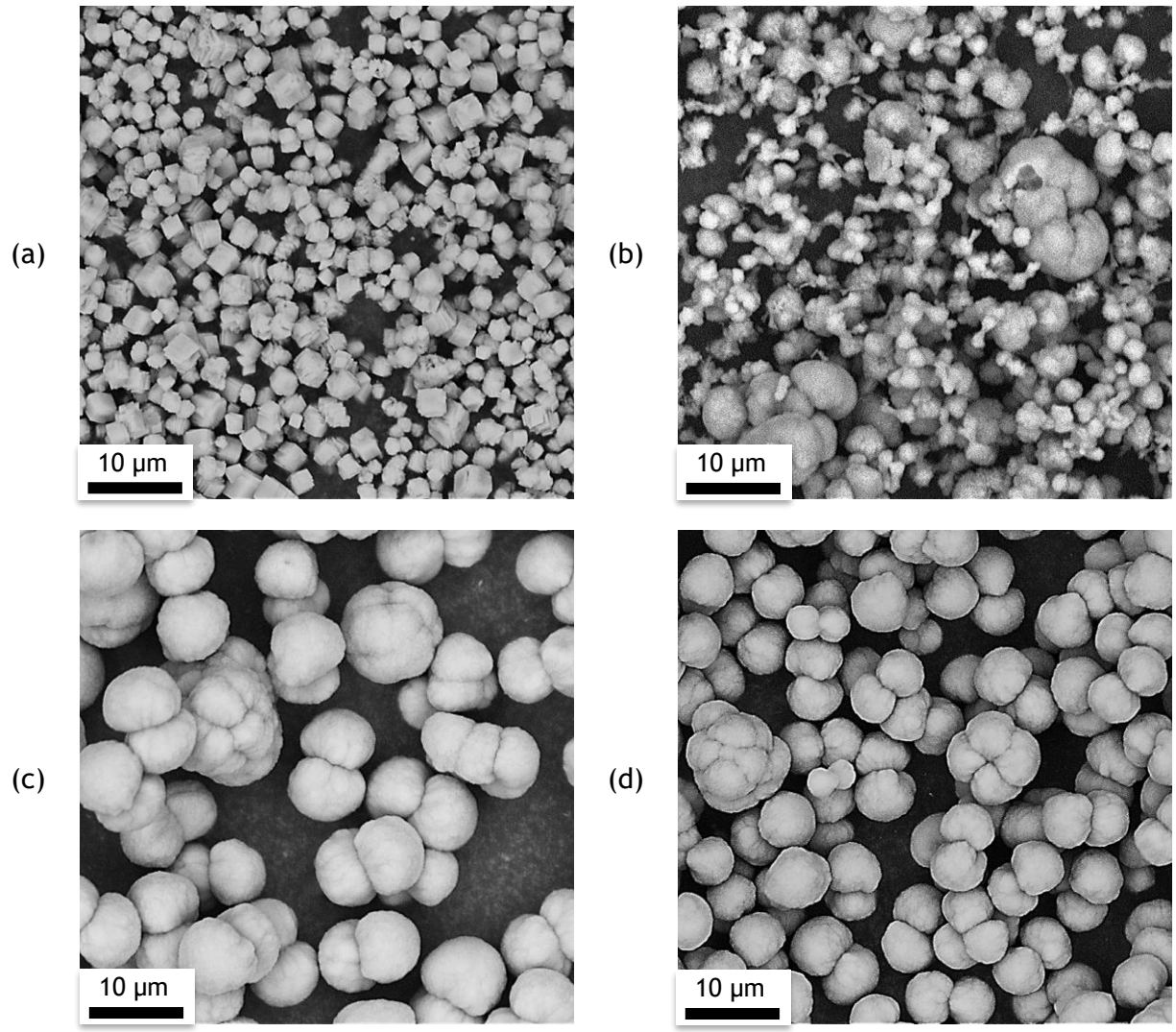

Figure 16 - SEM images of samples of the experiments (a) N01, (b) N02, (c) N03 and (d) N04.

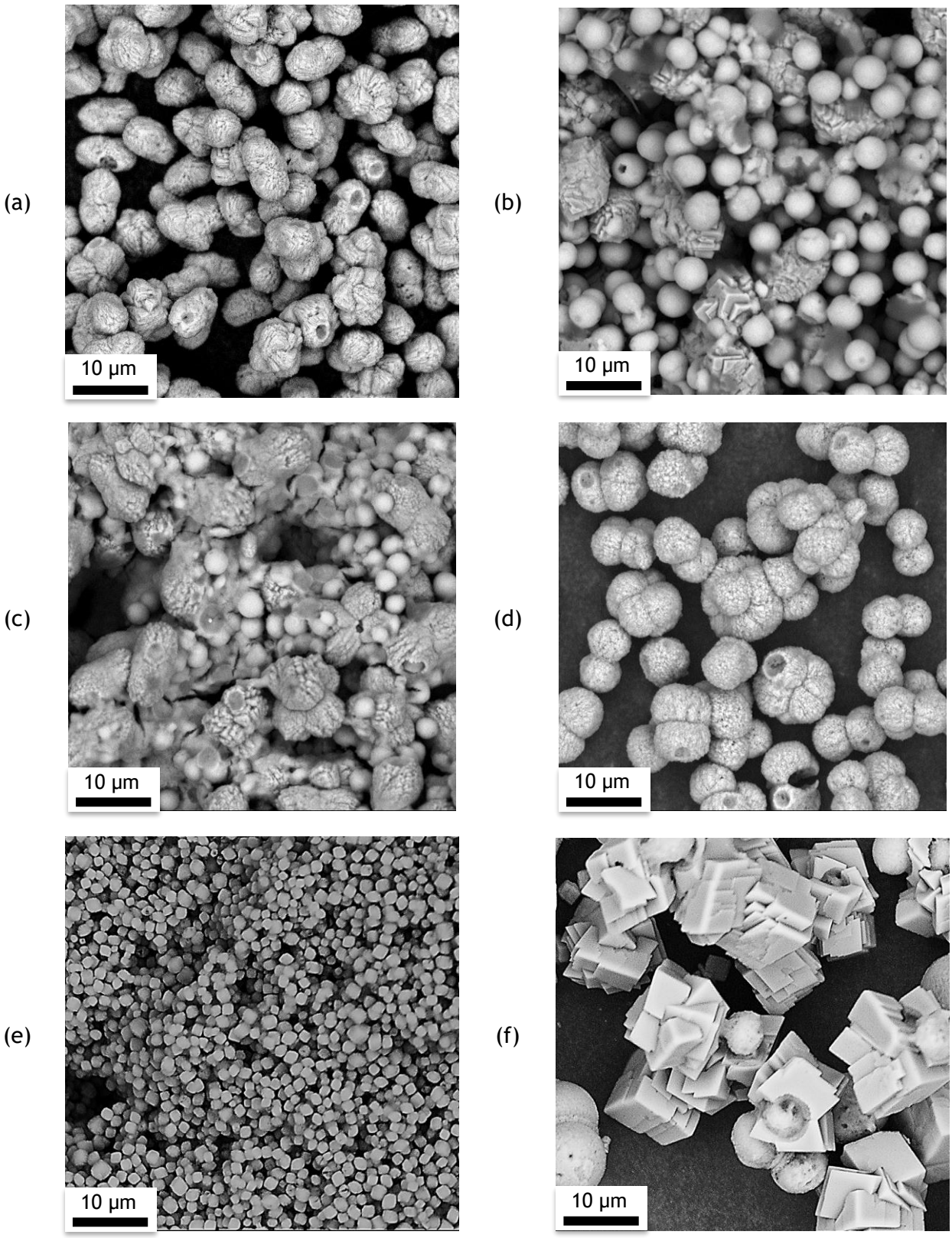

Figure 17 - SEM images of samples of the experiments (a) N05, (b) N06, (c) N07, (d) N08, (e) N09 and (f) N10.

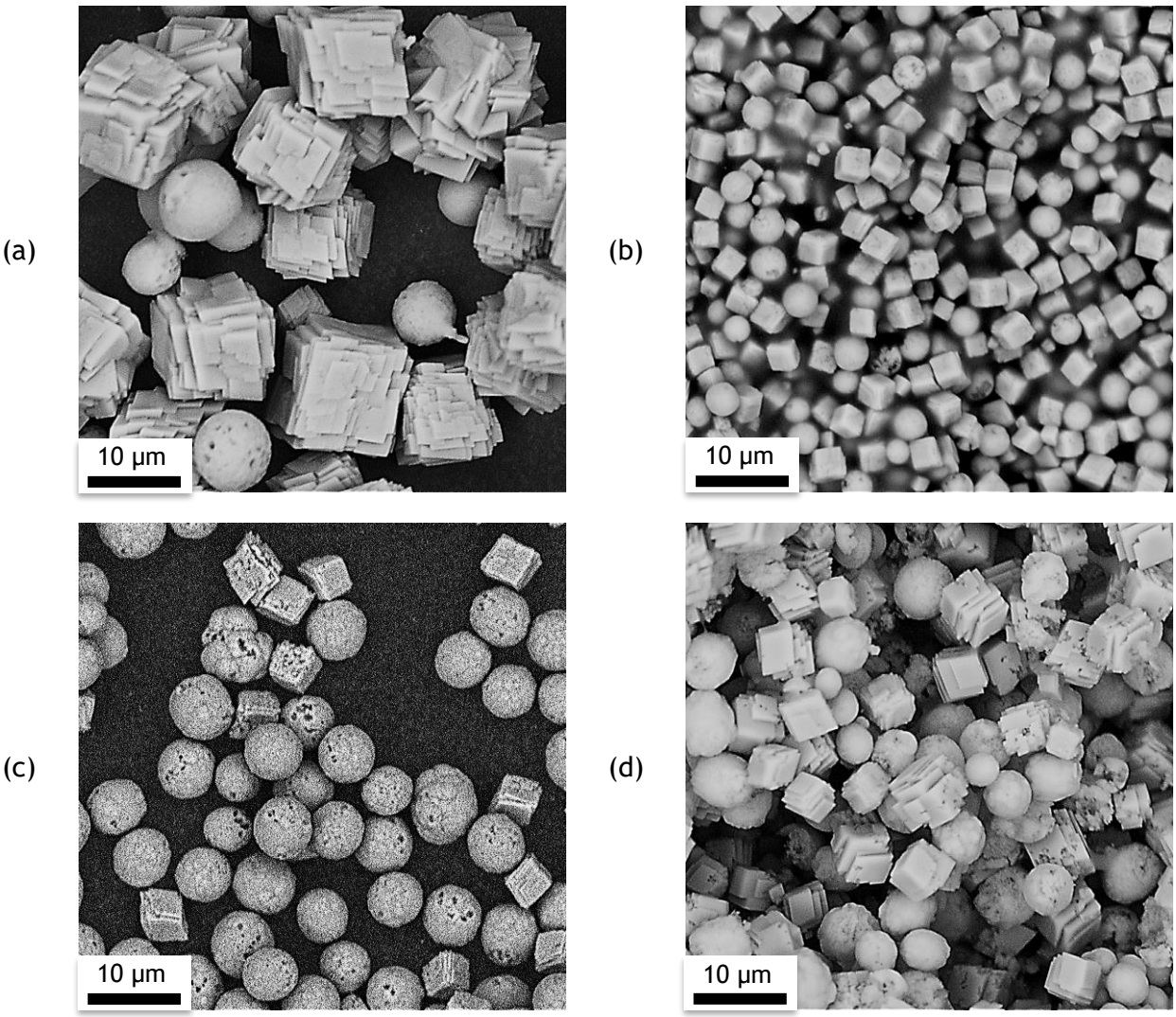

Figure 18 - SEM images of samples of the experiments (a) N11, (b) N12, (c) N13 and (d) N14.

For the first experiment performed in a continuous mode (N01) the reactants' concentration was set to 1 M, which resulted in a percentage of solids in the outlet close to the one in the semi-batch experiments. The Reynolds number was 400 and since that in the semi-batch experiments no dispersant was needed during the reaction, no sodium citrate or sodium oleate was added. However, as it can be seen from Figure 16a, the product obtained appears to be in a middle stage of recrystallization, containing particles that have already recrystallized and other that did not. Thus, it was concluded that the addition of a dispersant to the reactants, that would be present during the reaction, could be favourable. Therefore, for experiment N02, sodium citrate, equivalent to 4 layers, was added. It should be noted that since it was concluded, from the semi-batch experiments, that one layer of sodium citrate was not enough to provide the stability of the product, it was opted to use four times that amount. From Figure 16b, it is observable that no straight boundaries (indicatory of recrystallization) are present. Nevertheless, a high randomness of the particles' size and shape is verified. Moreover, it was observable that the outlet stream was too viscous (due to the presence of solids) and,

consequently, the Reynolds number inside the reactor could have decreased to a value below its critical. To solve this problem, the concentration of the reactants was set to 0.2 M, which would decrease the mass percentage of solids in the outlet to 1 % (experiment N03).

As it can be seen from Figure 16c, there was a clear improvement on the final product. The produced particles showed no evidence of straight boundaries. However, the formed clusters are visibly larger than those produced in the semi-batch experiments. To attack this problem, it was suggested to make the reaction happen faster, that is, with a smaller contact time between the reactants. For the purpose, a higher Reynolds number was used in experiments N04 and N05. Now, it was clearly visible, from Figure 16d, a decrease in the clusters' size (as a consequence of a higher Reynolds number). However, in Figure 17a, the size of the clusters did not change drastically, but the morphology of the product did (being formed from what appeared to be an aggregate of plate shaped particles).

Since it was shown that the addition of four layers of sodium citrate was enough to prevent recrystallization of the particles inside the NETmix, it made sense to evaluate if a smaller quantity would have the same effect. Thus, experiments N06 and N07 (with the equivalent to two and one layer of sodium citrate, respectively) were made. It can be seen, from Figure 17b and Figure 17c, that a smaller amount of dispersant was not enough, since the presence of recrystallized particles is clearly visible. Furthermore, and as expected, the level of recrystallization in experiment N07 is greater than that of experiment N06 (due to a smaller concentration of sodium citrate).

Experiment N08 was made with the intent of evaluating the effect of the reaction temperature in the final product. Comparing Figure 16d with Figure 17d, it can be seen that no significative change occurs.

A comparison between experiments N04, N09 and N10 allows conclusions to be taken about the effect of the use of dispersants during the reaction. When no dispersant is used (N10) the final product is highly irregular, being constituted by large particles of several shapes (Figure 17f). However, in the cases where a dispersant is used, the obtained product presents a much more uniform constitution (Figure 16d and Figure 17e). When sodium citrate is present during the reaction (Figure 16d) the clusters formed are of a large spherical shape and in the case of the dispersant being sodium oleate (Figure 17e), smaller aggregates with more square borders are formed.

With experiment N11 it was intended to conclude about the effect of the reaction temperature in the case where no dispersant was used. Now comparing Figure 17f and Figure 18a, no significant discrepancy was observed and so, it was inferred that the tested reaction temperatures were not a crucial aspect to the final product.

Comparing experiments N09 and N12, conclusions about the effect of the concentration of sodium oleate can be taken. Figure 17e (N09) shows a uniform product of relatively small size, as opposed to Figure 18b (N12), which presents a more random product of a more defined cubic shape. Since sodium oleate was expected to deagglomerate the calcium carbonate particles and prevent recrystallization, this result was not expected. Moreover, it was noticed that the solution of potassium carbonate containing the equivalent to four-layers of sodium oleate was fairly more viscous than water (the viscosity value considered). This may have induced errors in the calculation of the Reynolds number and, therefore, compromised the results.

Experiments N09 and N13 allow conclusions about the effect of the reactants' concentration. Figure 17e (N09) presents a more uniform product than the one obtained in experiment N13 (Figure 18c). However, in N13 it was verified that some particles passed through the filter paper. The filtered water presented a whitish colour, indicative of the presence of calcium carbonate particles. Since this had not happened in any other experiment, it is believable that clusters smaller than the pore size were formed. As already occurred in experiment N13, the potassium carbonate solution was clearly more viscous than water, which could have once more compromised the results.

At last, comparing experiments N13 and N14 (Figure 18c and Figure 18d, respectively), it can be concluded that higher Reynolds numbers are favourable to the formation of a more spherical shaped product, more similar to the one produced in the semi-batch experiment.

4.2.2 Transmission Electron Microscopy

As already happened with the batch obtained product, some samples were submitted to a TEM analysis. Figure 19, Figure 20 and Figure 21 show a set of TEM images of the calcium carbonate particles produced in the experiments N04, N09 and N13, respectively.

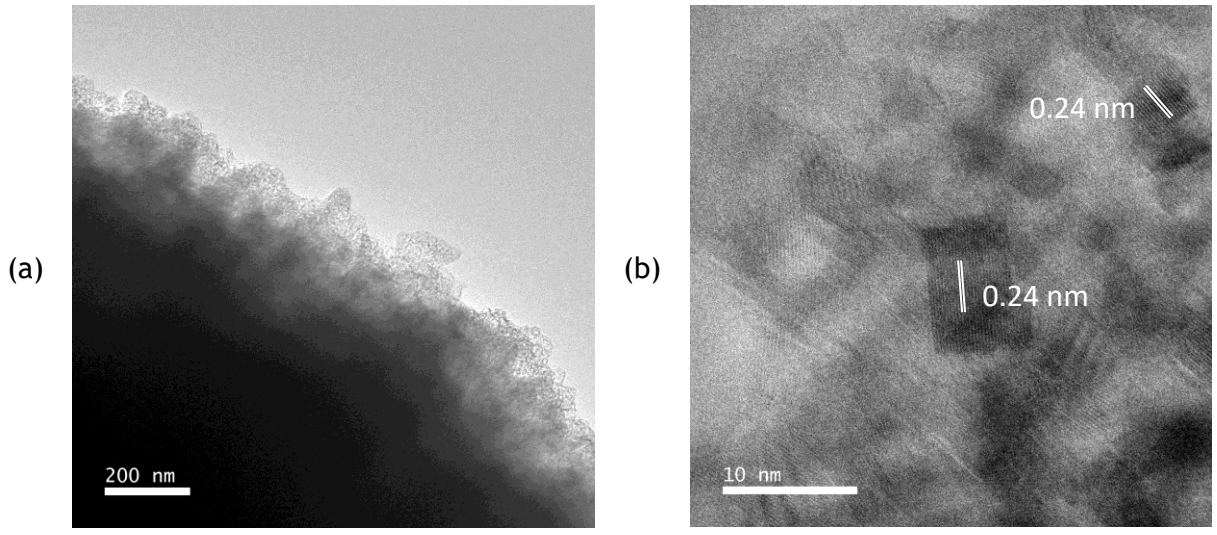

Figure 19 - TEM images of sample N04 with an ampliation of (a) 40k and (b) 1.2M times.

(a) 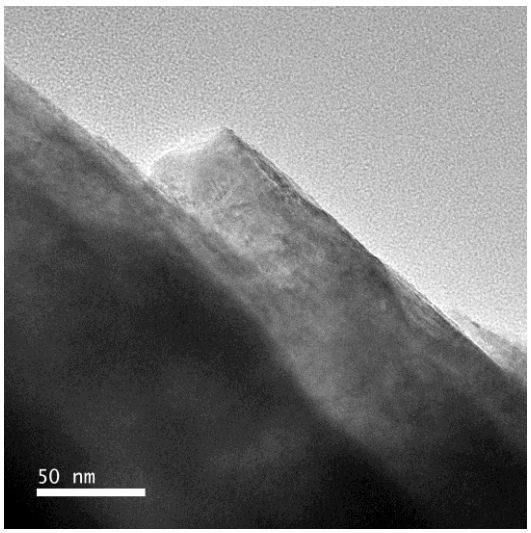

(b) 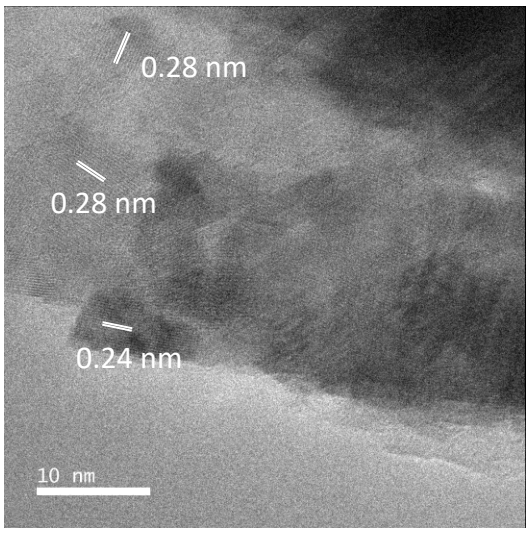

Figure 20 - TEM images of sample N09 with an ampliation of (a) 200k and (b) 1M times.

(a) 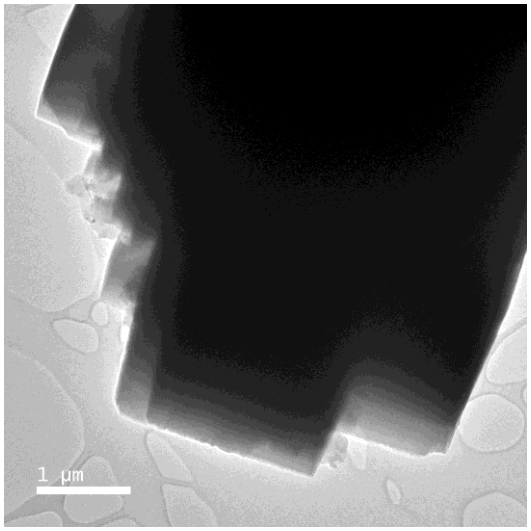

(b) 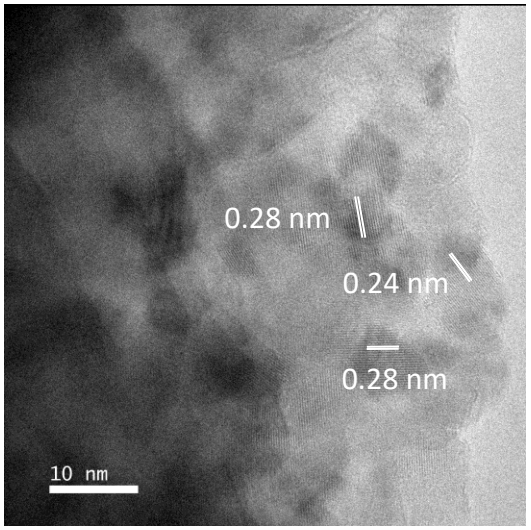

Figure 21 - TEM images of sample N13 with an ampliation of (a) 8k and (b) 800k times.

From Figure 19, it is possible to observe that the addition of sodium citrate during the reaction changes the morphology of the formed particles. However, the tendency they have to aggregate is such that their concrete morphology is unclear. Figure 19b presents clear patterns indicatory of crystalline structures.

The products seen in Figure 20 and Figure 21 were produced in the presence of sodium oleate. The change is evident: smoother boundaries are formed and the particles appear to be aggregated by a somewhat organized overlap of layers. Figure 20b and Figure 21b show striking evidence of crystalline structures.

Once again, the comparison of the fringe spacings measured with the data presented in Appendix B, allows the conclusion that aragonite δ_{200}, aragonite δ_{031} and calcite δ_{110} can exist due to the presence of the 0.24 nm fringe and aragonite δ_{002} or calcite δ_{006} can be represented

by the 0.28 nm fringe. These were the same polymorphs that were identified in the analysis of the batch product. Once more, the univocal identification of the phases was not possible.

More images of this analysis are presented in Appendix B.

4.2.3 Specific Surface Area

Once again, the specific surface area was determined (only for samples N04, N09 and N13) through the BET method. The same degassing condition was tested, and the nitrogen adsorption and desorption isotherms obtained are shown in Figure 22.

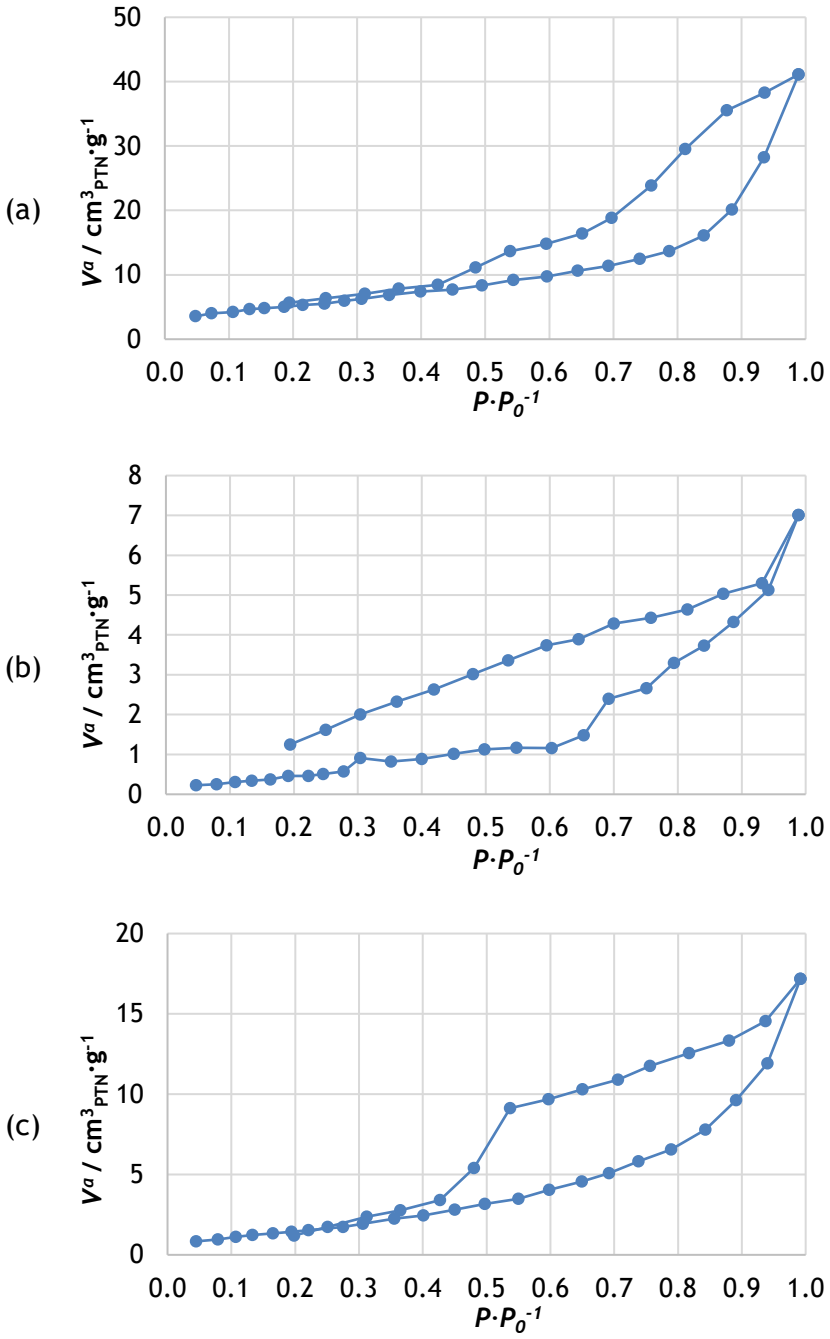

Figure 22 – Nitrogen adsorption and desorption isotherms for experiment (a) N04, (b) N09 and (c) N13.

The isotherms from Figure 22 correspond, once more, to non-porous or macro-porous materials that present a multilayer confined adsorption, where its hysteresis is typical of aggregates of particles with a platelet structure that form slit-like pores (like in the product from the batch experiment). The loop seen in Figure 22a and Figure 22c likely results from capillary condensation in the slits between the particles that constitute the pores and the blockage effect observed can suggest a random arrangement of the particles.

Table 7 summarizes the BET surface areas obtained as well as the equivalent particle radius, r. This last value was once more calculated assuming a spherical geometry and the density of calcite.

Table 7 - BET surface area and respective radius of the calcium carbonate particles of the NETmix experiments.

Degassing conditions	Experiment	S_{BET} / $\mathbf{m^2 \cdot g^{-1}}$	r / nm
120 ºC for 3 hours	N04	18.9	59
	N09	2.2	503
	N13	6.2	179

Once again, the calculated particle radii were not smaller than 50 nm. However, and as seen in the above presented results, this type of analysis can be unsuitable for the determination of the surface area of these products (due to the high tendency for agglomeration of the particles). Therefore, no significative conclusions can be taken from this analysis.

4.2.4 Fourier-Transform Infrared Spectroscopy (FTIR)

FTIR analysis was performed with the intent of finding out if the surface treatment made with sodium citrate or sodium oleate altered the type of polymorph being produced. In that sense, samples from experiment N04 and N09 were analysed and the obtained spectrums are presented in the figure below.

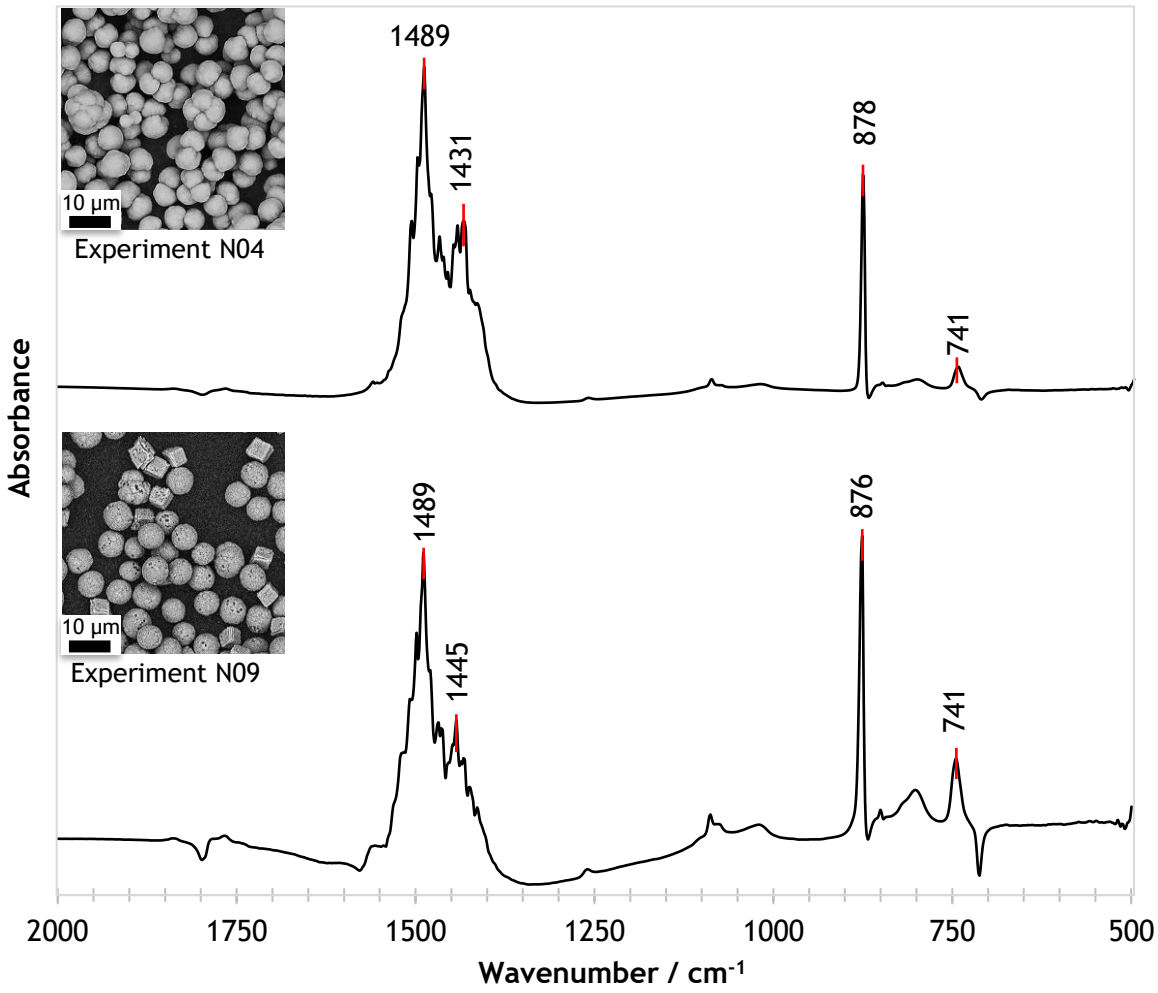

Figure 23 - FTIR spectra for the calcium carbonate particles produced in experiment N04 and N09.

As it can be seen from Figure 23, the peaks obtained for the two samples are very similar to the ones obtained in Figure 15 and correspond to vaterite. Once more, this result discords with the more reliable TEM report and, therefore, it is concluded that this type of analysis is not indicated to distinguish between the different types of polymorphs.

5 Economic Analysis

In this chapter, a preliminary economic assessment for a production plant of calcium carbonate was made. Initially, the process was simulated in Aspen Plus V9 and then, the data obtained was sent to Aspen Process Economic Analyzer (APEA) where the economic analysis was performed. Results are presented below.

5.1 Aspen Plus Simulation

As mentioned, the first step for the economic assessment of the process consisted in the simulation in Aspen Plus. Figure 24 shows a simplified flowsheet of the simulated process.

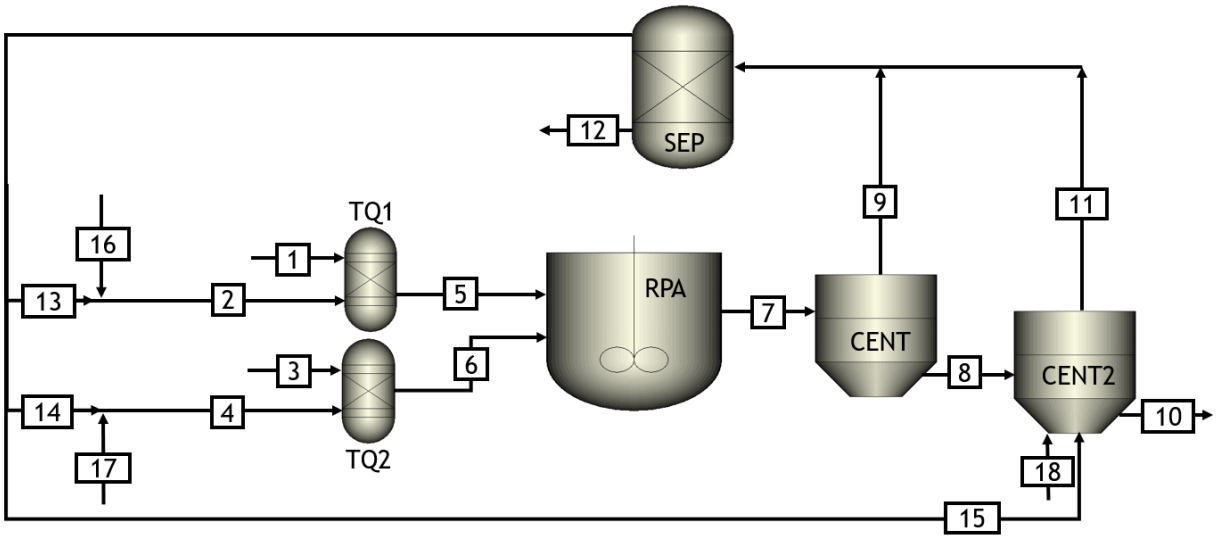

Figure 24 – Simplified flowsheet of the simulated process for the production of calcium carbonate.

As it can be seen from Figure 24, initially the reactants (streams 1 and 3) are feed, along with water, to blocks TQ1 and TQ2, where the dissolution of the salts happens. It should be noted that in this simulation the concentration of the reactants was set to 0.2 M, which resulted in a mass fraction of calcium carbonate in the outlet stream of the reactor (stream 7) of 1 % (the same value as in the majority of the NETmix experiments).

Afterwards, the reactants' solutions are pumped into the RPA block, which simulates the NETmix reactor, operating at atmospheric pressure and ambient temperature. Furthermore, the reactor was simulated using the same residence time as in the experiments whose Reynolds number was 650 and, since the occurring reaction is a precipitation, the conversion of the reactants was approximately one (0.999).

Following this, stream 7 is directed towards a centrifuge, where the product is concentrated, and the potassium chloride formed during the reaction and dissolved in the water is majorly removed. The calcium carbonate rich stream (stream 8) now contains about 16.6 % w/w calcium carbonate and follows into another centrifuge, after the addition of clean water (streams 15 and 18). This last step is necessary to further remove the potassium chloride formed in the reaction. It must be highlighted the fact that a 5 % loss of the calcium carbonate is experienced in each one of the centrifuges and that the final product (stream 10) consists in a slurry with ca. 16.6 % w/w of solid calcium carbonate with a purity greater than 99 %.

Another case test consisted in the economic analysis for the case of a 10 % loss of calcium carbonate in each centrifuge. It was not observed a significative change in the final result and, therefore, a 5 % loss for each equipment was considered.

Since the molar concentration of the reactants is relatively low, the need for water in the process is elevated and the treatment and reuse of the same becomes crucial. In that sense, the removed water in the centrifuges (streams 9 and 11) is submitted to a filtration (to remove the calcium carbonate), an ultraviolet treatment and to reverse osmosis (to remove the dissolved potassium chloride). Since this type of treatments are not possible to simulate using Aspen Plus, it was considered that 5 % of the potassium chloride passed to the clean stream of water and that 10 % of the water was lost.

Finally, the reactants and water flow rates were evened so that 600 $kg \cdot h^{-1}$ of a slurry of ca. 17 % of calcium carbonate (the equivalent to 100 $kg \cdot h^{-1}$ of solid calcium carbonate) were produced. It must be referred that other productions, both to higher and lower values, were tested and that this value was deemed the most reasonable in terms of the compromise of the equipment's dimensions and total production for a start-up company. Therefore, it was the production considered for the following analysis.

It should be pointed out that the addition of dispersants was not considered in the Aspen simulation here shown and nor in the cost analysis below presented. However, these costs were calculated, and it was concluded that they had an insignificant impact on the final results of the analysis.

In Appendix C, a more detailed flowsheet of the process is shown, as well as a table with the composition of the more important streams of the process.

5.2 Aspen Process Economic Analyzer (APEA)

After the simulation performed in Aspen Plus, the results of the mass balance obtained are exported to Aspen Process Economic Analyzer (APEA), which will, after the sizing of the equipment, proceed to an economic evaluation of the process.

Initially, it was defined that the process to evaluate would be a new process located in Europe and that the estimated start date for the basic engineering would be 1 of January of 2019. The labouring force was taken as one shift constituted by 1 supervisor (that costed 35 €/hour) and 3 operators (for 20 €/hour each) and the standard work week was considered to be of 40 hours.

The economic life of the project, that is, the time over which capital costs will be depreciated was fixed in 5 years and escalation was defined as 5 % per year for the project capital and products, 3.5 % per year for raw material and 3 % per year for operating and maintenance labour and utilities.

The raw materials cost was defined as presented in Table 8.

Table 8 - Cost of the raw materials for the production of calcium carbonate [46, 47].

Raw material	Cost / €·kg^{-1}
$CaCl_2$	0.25
K_2CO_3	0.71
H_2O	2.6×10^{-3}

It is important to note that although the costs presented in Table 8 were the considered in the analysis described below, they can be changed at any time. In the future, a more profound market assessment for these compounds will have to be made in order to produce a more realistic economic assessment.

Afterwards, the software proceeded to the automatic sizing of the equipment. Stainless steel 316 (SS316) was defined as the construction material for all equipment and the storage tanks volumes were calculated as described in Appendix C. In this appendix, the dimensions of the equipment, calculated by APEA, are also presented.

Table 9 shows the equipment's descriptions and its respective calculated price.

Table 9 - Description of the equipment of the process and respective costs associated.

Equipment	Corresponding Block	Description	Cost / €
Stirring tank	TQ1	Agitated tank (open top)	169 800
	TQ2	Agitated tank (open top)	169 800
	RPA	Agitated tank (open top)	127 600
Pump	P1 to P12	Centrifuge single or multi-stage pump	496 600
Centrifuge	CENT and CENT2	Solid bowl centrifuge	484 800
Storage tank for $CaCO_3$ suspension	-	Vertical process vessel	342 900
Storage tank for water	-	Vertical process vessel	266 800
Reverse Osmosis Unit	-	-	32 400

Therefore, the total equipment cost amounts to a total of, approximately, 2.1 M€. It should be noted that the same equipment, when constructed in carbon steel, would cost a total of 1.5 M€, which would represent a decrease of about 29 %.

Finally, the yearly hours of production were defined, and an automatic economic analysis was performed by the software. Three distinct production cases were studied: for a production of 1500 h per year (the equivalent of 100 % of the production capacity of the sized plant); for 750 h per year (50 % of the production capacity); and 375 h per year (25 % of the production capacity). Table 10 lists the main results obtained from this analysis for the three cases studied.

Table 10 – Economic analysis summary.

	Production capacity / %		
	100	**50**	**25**
Total Project Capital Cost / M€	7.92		
Total Operating Cost / M€ per year	0.64	0.51	0.44
Price of the $CaCO_3$ suspension / €·kg^{-1}	5.4	10.5	20.5
Price of the solid $CaCO_3$ / €·kg^{-1}	32.5	63.2	123.5

It should be noted that the prices described in the table correspond to the prices at which the calcium carbonate (solid or in a slurry) must be sold for the investment to be returned in 5 years, that is, the price that makes the payback time of the project equal to 5 years.

From Table 10, it should be retained that the capital cost for all cases studied is the same, since a unique industrial installation was dimensioned and the only difference consists in the

hours of production. A more detailed description for this type of costs is presented in Appendix C.

The operation costs, as expected, decrease when lower production hours in a year are used and the price at which the calcium carbonate slurry has to be sold for the investment to be returned in 5 years increases. For a full capacity of the installation (a yearly production of 900 tons), the calcium carbonate slurry must be sold at 5.4 €·kg^{-1} (the equivalent of 32.5 €·kg^{-1} of solid calcium carbonate). This price raises for 10.5 €·kg^{-1} when the capacity is at 50 % (450 tons per year) and to 20.5 €·kg^{-1} when it is at 25 % (225 tons per year).

As means of comparison, it is important to know that the commercial price of the dried compound is evaluated between 12 to 69 €·kg^{-1} for the nanoproduct [46, 48] and at about 112 €·kg^{-1} for when the product is in a water suspension of about 40 % w/w [49].

Further optimization of this analysis can be made by verifying the costs assumed for the raw materials and optimizing the operating conditions of the process.

6 Conclusion

In terms of conclusions, this thesis can be divided into two main studies: the stability of the produced particles over time when stored under different conditions and the influence of certain variables, when using the NETmix reactor for continuous flow production, on the final product.

For the first study, the product was produced in a semi-batch reactor and stored under different conditions. Analyses were performed periodically to analyse if the produced particles remained of the same size and morphology as in its production day. It was concluded that when the particles were stored in distilled water, they completely recrystallized after one week. However, the addition of dispersants clearly improved this aspect, as sodium oleate allowed the stability of the product for, at least, 16 weeks. The addition of sodium citrate also had a positive outcome, although the recrystallization occurred within 16 weeks. It was also shown that lower temperatures retarded the recrystallization process and that a two-layer solution of sodium citrate was more effective in the inhibition of the recrystallization of the particles than a one-layer solution of the same dispersant.

With the respect to the study of the influence of certain process variables in the final product produced through the NETmix technology, it can be concluded that, for the recrystallization not to occur inside the NETmix, it is necessary to add the dispersants directly to the reactants (so that the compound is present during the reaction) and that the reaction temperatures tested had no significative effect on the final product.

In the experiments performed with the sodium citrate dispersant, it was verified that less than four layers of dispersant were not enough to produce spherical particles and that higher Reynolds numbers produced smaller clusters of spherical particles, but when this number increased significantly the morphology of the produced particles changed.

For the sodium oleate experiments, it was also verified that higher Reynolds numbers favoured the formation of more spherical particles and that a higher concentration of reactants produced a less uniform product. It was also seen that an increase in the mass of dispersant did not produce smaller particles, as expected. However, it is important to highlight that, in experiments N12 through N14, there was an apparent increase in the viscosity of the potassium carbonate and sodium oleate solution, which could have compromised the results.

At last, a preliminary economic analysis for a production process of calcium carbonate was made using the Aspen Plus and the Aspen Process Economic Analyzer software. It was concluded that the price at which the produced product would have to be sold for the investment to be returned in 5 years was 5.4 €·kg^{-1} (for a full production capacity of the sized plant).

7 Assessment of the Work Done

7.1 Objectives Achieved

In the beginning of this work it was set that the main objective consisted in the continuous production of nanoparticles and microparticles of calcium carbonate using the NETmix technology. In this sense, experiments in a semi-batch set-up and in the NETmix reactor were carried out. Although the final product of the NETmix experiments is not quite the same as the one obtained in the semi-batch set-up, clear improvements were made since the first NETmix experiments. Besides that, the effect of certain process variables in the final product were studied and comprehended, as set out in the beginning of this work.

Furthermore, the study of different storage conditions in the stability of the produced particles over time was also successfully evaluated.

7.2 Limitations and Future Work

Due to time limitations, the influence of certain process variables, such as the pH medium, in the formed product have yet to be evaluated. Furthermore, future work can include parameter optimization for the NETmix process and for both the cases where the sodium citrate and sodium oleate are used as dispersants. However, in the case of the sodium oleate being present during the reaction, rheological tests will be necessary to evaluate the viscosity of the mixture of this dispersant with potassium carbonate, which, as mentioned, appeared to significantly vary from the considered viscosity of the water and may have, consequently, compromised these results.

Moreover, an XRD analysis would have to be performed for a univocal phase identification of the calcium carbonate produced.

Additionally, in the batch experiments, it would be interesting to study the effect of other reaction temperatures in the final product and to verify the efficiency of the storage conditions for a higher concentration of solids. The analysis of the effect of the use of other reactants would also be relevant.

The evaluation of the qualities of the product in certain common applications would also constitute an interesting task to develop in the future.

References

1. Köhler, M. and W. Fritzsche, *Nanotechnology: An Introduction to Nanostructuring Techniques*. 2007: Wiley-VCH Verlag GmbH & Co. KGaA.
2. Rao, C.N.R., A. Müller, and A.K. Cheetham, *The Chemistry of Nanomaterials: Synthesis, Properties and Applications*. Vol. 1. 2004: WILEY-VCH Verlag GmbH & Co. KGaA.
3. Bhushan, B., *Introduction to Nanotechnology*, in *Handbook of Nanotechnology*. 2010, Springer.
4. Park, K., *Nanotechnology: What it can do for drug delivery*, N.I.o. Health, Editor. 2007: Journal of controlled release : official journal of the Controlled Release Society.
5. Tolfree, D. and M.J. Jackson, *Commercializing Micro-Nanotechnology Products*. 2008: CRC Press - Taylor & Francis Group, LLC.
6. Bueno, P.R. and C. Gabrielli, *Electrochemistry, Nanomaterials, and Nanostructures*, in *Handbook of Nanostructured Materials for Alternative Energy Devices*. 2014, SPRINGER. p. 81-149.
7. Blue, C.R., A. Giuffre, S. Mergelsberg, N. Han, J.J. De Yoreo, and P.M. Dove, *Chemical and physical controls on the transformation of amorphous calcium carbonate into crystalline CaCO3 polymorphs*. Geochimica et Cosmochimica Acta, 2017. **196**: p. 179-196.
8. Chaussemier, M., E. Pourmohtasham, D. Gelus, N. Pecoul, H. Perrot, J. Ledion, H. Cheap-Charpentier, and O. Horner, *State of art of natural inhibitors of calcium carbonate scaling. A review article*. Desalination, 2015. **356**: p. 47-55.
9. He, M., B.U. Cho, and J.M. Won, *Effect of precipitated calcium carbonate--Cellulose nanofibrils composite filler on paper properties*. Carbohydr Polym, 2016. **136**: p. 820-5.
10. Kanoje, B., D. Patel, and K. Kuperkar, *Morphology modification in freshly Precipitated Calcium Carbonate particles using surfactant-polymer template*. Materials Letters, 2017. **187**: p. 44-48.
11. Savelyeva, M.S., A.A. Abalymov, G.P. Lyubun, I.V. Vidyasheva, A.M. Yashchenok, T.E. Douglas, D.A. Gorin, and B.V. Parakhonskiy, *Vaterite coatings on electrospun polymeric fibers for biomedical applications*. J Biomed Mater Res A, 2017. **105**(1): p. 94-103.
12. Shimpi, N., A. Mali, D.P. Hansora, and S. Mishra, *Synthesis and Surface Modification of Calcium Carbonate Nanoparticles Using Ultrasound Cavitation Technique*. Nanoscience and Nanoengineering, 2015. **3**(1): p. 8-12.
13. Carr, F.P., D.K. Frederick, and U.b. Staff, *Calcium Carbonate*, in *Kirk-Othmer Encyclopedia of Chemical Technology*. 2014, John Wiley & Sons, Inc. p. 1-7.
14. Thenepalli, T., A.Y. Jun, C. Han, C. Ramakrishna, and J.W. Ahn, *A strategy of precipitated calcium carbonate (CaCO3) fillers for enhancing the mechanical properties of polypropylene polymers*. Korean Journal of Chemical Engineering, 2015. **32**(6): p. 1009-1022.
15. Biradar, S., P. Ravichandran, R. Gopikrishnan, V. Goornavar, J.C. Hall, V. Ramesh, S. Baluchamy, R.B. Jeffers, and G.T. Ramesh, *Calcium carbonate nanoparticles: synthesis, characterization and biocompatibility*. Journal of Nanoscience and Nanotechnology, 2011. **11**(8): p. 6868-6874.
16. Schmid, G., *Nanoparticles: from theory to application*. 2004: WILEY-VCH Verlag GmbH & Co. KGaA.

17. Hummel, R.E., *The Wave-Particle Duality*, in *Electronic Properties of Materials*. 2011. p. 7-14.

18. Feng, B., A.K. Yong, and H. An, *Effect of various factors on the particle size of calcium carbonate formed in a precipitation process.* Materials Science and Engineering a-Structural Materials Properties Microstructure and Processing, 2007. **445**: p. 170-179.

19. Lee, I., S.W. Han, H.J. Choi, and K. Kim, *Nanoparticle-Directed Crystallization of Calcium Carbonate.* Advanced Materials, 2001. **12**(21): p. 1617-1620.

20. Kitamura, M., *Crystallization and Transformation Mechanism of Calcium Carbonate Polymorphs and the Effect of Magnesium Ion.* J Colloid Interface Sci, 2001. **236**(2): p. 318-327.

21. Leeuw, N.H.d. and S.C. Parker, *Surface and Morphology of Calcium Carbonate Polymorphs Calcite, Aragonite, and Vaterite: An Atomistic Approach.* Journal of Physical Chemistry B, 1998. **102**(16): p. 2914-2922.

22. Raiteri, P. and J.D. Gale, *Water Is the Key to Nonclassical Nucleation of Amorphous Calcium Carbonate.* Journal of the American Chemical Society, 2010. **132**(49): p. 17623-17634.

23. Global Industry Analysts, I. *The Global Calcium Carbonate Market: Trends, Drivers & Projections.* 2015 [cited 2018, 14 March]; Available from: http://www.strategyr.com/MarketResearch/Calcium_Carbonate_Market_Trends.asp.

24. Alua, P.M.N.d.C., *Optimização da opacidade de tintas aquosas*, in *Departamento de Engenharia Química*. 2012, Universidade Técnica de Lisboa. p. 131.

25. Gorna, K., M. Hund, M. Vucak, F. Grohn, and G. Wegner, *Amorphous calcium carbonate in form of spherical nanosized particles and its application as fillers for polymers.* Materials Science and Engineering a-Structural Materials Properties Microstructure and Processing, 2008. **477**(1-2): p. 217-225.

26. Kenny, M. and T. Oates, *Lime and Limestone*, in *Ullmann's Encyclopedia of Industrial Chemistry*. 2007.

27. Sukhorukov, G.B., D.V. Volodkin, A.M. Gunther, A.I. Petrov, D.B. Shenoy, and H. Mohwald, *Porous calcium carbonate microparticles as templates for encapsulation of bioactive compounds.* Journal of Materials Chemistry, 2004. **14**(14): p. 2073-2081.

28. Trushina, D.B., T.V. Bukreeva, M.V. Kovalchuk, and M.N. Antipina, *CaCO3 vaterite microparticles for biomedical and personal care applications.* Mater Sci Eng C Mater Biol Appl, 2014. **45**: p. 644-58.

29. Radha, A.V., T.Z. Forbes, C.E. Killian, P.U. Gilbert, and A. Navrotsky, *Transformation and crystallization energetics of synthetic and biogenic amorphous calcium carbonate.* Proc Natl Acad Sci U S A, 2010. **107**(38): p. 16438-43.

30. Rodriguez-Blanco, J.D., S. Shaw, P. Bots, T. Roncal-Herrero, and L.G. Benning, *The role of pH and Mg on the stability and crystallization of amorphous calcium carbonate.* Journal of Alloys and Compounds, 2012. **536**: p. S477-S479.

31. Lopez-Arce, P., L.S. Gomez-Villalba, S. Martinez-Ramirez, M.A. de Buergo, and R. Fort, *Influence of relative humidity on the carbonation of calcium hydroxide nanoparticles and the formation of calcium carbonate polymorphs.* Powder Technology, 2011. **205**(1-3): p. 263-269.

32. Vagenas, N.V., A. Gatsouli, and C.G. Kontoyannis, *Quantitative analysis of synthetic calcium carbonate polymorphs using FT-IR spectroscopy.* Talanta, 2003. **59**(4): p. 831-836.

33. Gehrke, N., H. Cölfen, N. Pinna, M. Antonietti, and N. Nassif, *Superstructures of Calcium Carbonate Crystals by Oriented Attachment*. Crystal Growth and Design, 2005. **5**(4): p. 1317-1319.

34. Ogino, T., T. Suzuki, and K. Sawada, *The formation and transformation mechanism of calcium carbonate in water*. Geochimica et Cosmochimica Acta, 1987. **51**(10): p. 2757-2767.

35. Teir, S., S. Eloneva, C.J. Fogelholm, and R. Zevenhoven, *Dissolution of steelmaking slags in acetic acid for precipitated calcium carbonate production*. Energy, 2007. **32**(4): p. 528-539.

36. Kitamuraa, M., H. Konnob, A. Yasuia, and H. Masuokaa, *Controlling factors and mechanism of reactive crystallization of calcium carbonate polymorphs from calcium hydroxide suspensions*. Journal of Crystal Growth, 2002. **236**: p. 323–332.

37. Said, A., H.P. Mattila, M. Jarvinen, and R. Zevenhoven, *Production of precipitated calcium carbonate (PCC) from steelmaking slag for fixation of CO2*. Applied Energy, 2013. **112**: p. 765-771.

38. Lopes, J.C.B., P.E.M.d.S.d. Laranjeira, Costa, M.M.G.Q. Dias, and A.A.A. Martins, *Network Mixer and Related Mixing Process*, in *US Patent*. 2013.

39. Gomes, P.J., V.M.T.M. Silva, P.A. Quadros, M.M. Dias, and J.C.B. Lopes, *A Highly Reproducible Continuous Process for Hydroxyapatite Nanoparticles Synthesis*. Journal of Nanoscience and Nanotechnology, 2009. **9**(6): p. 3387-3395.

40. Costa, M.F.d.S., *Development of Nanomaterials using the NETmix® Technology: Application to Production of MOFs*, in *Departamento de Engenharia Química*. 2012, Faculdade de Engenharia da Universidade do Porto.

41. Laranjeira, P.E., A.A. Martins, J.C.B. Lopes, and M.M. Dias, *NETmix®, a new type of static mixer: Modeling, simulation, macromixing, and micromixing characterization*. AIChE Journal, 2009. **55**(9): p. 2226-2243.

42. Laranjeira, P.E., A.A. Martins, M.I. Nunes, J.C.B. Lopes, and M.M. Dias, *NETmix®, a new type of static mixer: Experimental characterization and model validation*. AIChE Journal, 2011. **57**(4): p. 1020-1032.

43. National Center for Biotechnology, I. *PubChem Compound Database; CID=23665730*. [cited 2017, 17 December]; Available from: https://pubchem.ncbi.nlm.nih.gov/compound/23665730

44. National Center for Biotechnology, I. *PubChem Compound Database; CID=6224*. [cited 2017, 17 December]; Available from: https://pubchem.ncbi.nlm.nih.gov/compound/6224.

45. *Coulter LS Series: Product Manual*. 2011, Beckman Coulter, Inc.

46. Reed Business, I. *Indicative Chemical Prices*. 2006 [cited 2018, 15 May]; Available from: https://www.icis.com/chemicals/channel-info-chemicals-a-z/.

47. *Tarifário Águas do Porto (Aprovado em Reunião de Executivo da CMP em 21/12/2017)*. 2018.

48. US Research Nanomaterials, I. *Precipitated Calcium Carbonate Nanoparticles / CaCO3 Nanopowder, 50nm, 98%*. [cited 2018, 20 June]; Available from: https://www.us-nano.com/inc/sdetail/34312.

49. US Research Nanomaterials, I. *Precipitated Calcium Carbonate Nanoparticles / CaCO3 Nanopowder, 50nm, 40wt%, Water Dispersion*. [cited 2018, 20 June]; Available from: https://www.us-nano.com/inc/sdetail/34324.

50. *Zetasizer NanoSeries: User Manual*, in *MAN0317*. 2009, Malvern Instruments Ltd.

51. Swapp, S. *Scanning Electron Microscopy (SEM)*. Geochemical Instrumentation and Analysis [cited 2018, 10 April]; Available from: https://serc.carleton.edu/research_education/geochemsheets/techniques/SEM.html.

52. Goodge, J. *Energy-Dispersive X-Ray Spectroscopy (EDS)*. [cited 2018, 10 April]; Available from: https://serc.carleton.edu/research_education/geochemsheets/eds.html.

53. Stuart, B., *Infrared Spectroscopy: Fundamentals and Applications*. Analytical Techniques in the Sciences. John Wiley & Sons.

54. Al Omari, M.M., I.S. Rashid, N.A. Qinna, A.M. Jaber, and A.A. Badwan, *Calcium Carbonate*. Profiles Drug Subst Excip Relat Methodol, 2016. **41**: p. 31-132.

55. Williams , D.B.C., C. Barry, *Transmission Electron Microscopy: A Textbook for Materials Science*. 2009, Springer.

Appendix A. Characterization Techniques

In the subsections below, a brief description of the techniques that were used to characterize the product is made.

A.1 Laser Diffraction for Particle Size Analysis

In the diffraction method, the laser beam illuminates the sample, which scatters the light in patterns according to the size of its constituting particles. Posteriorly, Fourier optics collect the diffracted light and focus it on three sets of detectors (for low-angle scattering, mid-angle scattering and high angle scattering). However, for particles smaller than 0.4 μm it is very difficult to distinguish particles of different sizes by diffraction patterns alone and, therefore, the PIDS method is often jointly employed. It is based in a property of light called polarization and consists in the illumination of the sample particles with beams of light polarized vertically and then horizontally (relatively to the plane containing the light source, scattering region and detectors). Posteriorly, the difference in the scattered intensity between the vertical and horizontal polarizations as a function of the angle is determined since it depends on the ratio of the particle size to the wavelength of the light wave.

A.2 Electrophoresis and Laser Doppler Velocimetry (LDV)

A charged particle, suspended in a liquid, will attract ions of the opposite charge to its surface. The liquid layer surrounding the particle will, therefore, be constituted by two distinct parts: an inner region – the stern layer – where the ions are strongly bound and an outer region, diffuse layer, where they are more loosely bound. Thus, an electrical double layer exists around each particle (see Figure 25). In the diffusive layer there is a boundary inside of which the ions and particles form a stable entity, meaning that when a particle moves, ions within the boundary move with it, but any ions beyond the boundary do not go with the particle. This boundary is the so called slipping plane and the potential in this point is called the zeta potential [50].

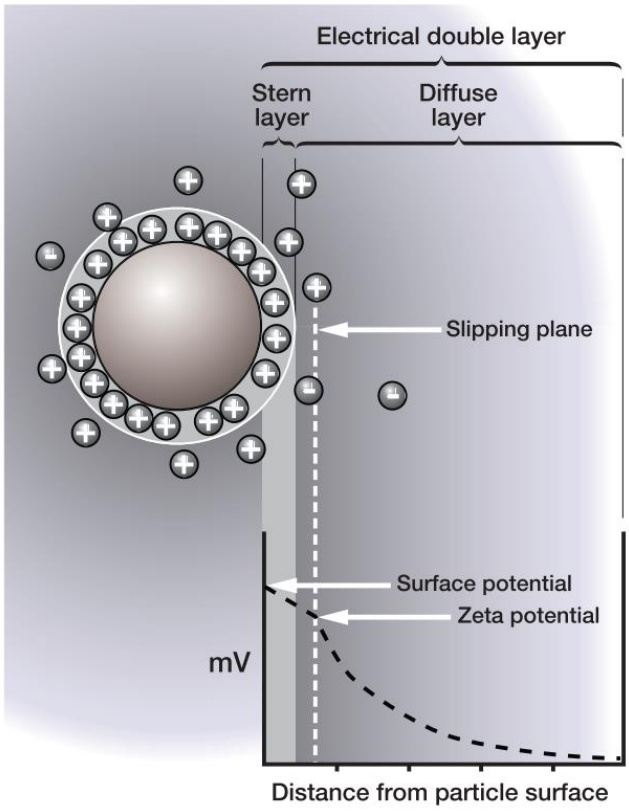

Figure 25 - Electrical double layer on the particle's surface [50].

The absolute value of the zeta potential points to the stability of the system. If the absolute value is large (greater than +30 mV or smaller than -30 mV), the particles in the suspension will tend to repel each other and there will be no tendency to flocculate. However, in the case of low values of the zeta potential (between -30 mV and +30 mV) there is no force to prevent the particles from agglomerating and flocculating. In the first case, the suspension is considered stable and in the second one, unstable [50].

The potential zeta value is measured using a combination of the electrophoresis and laser Doppler velocimetry (LDV) techniques. Electrophoresis is defined as the movement of a charged particle relative to the liquid it is suspended in under the influence of an applied electric field. The velocity of the particles is often called the electrophoretic mobility and it is related to the zeta potential and constants of the sample (such as viscosity and dielectric constant) by the Henry equation. Therefore, the knowledge of this velocity allows the knowledge of the zeta potential value. With that purpose, the LDV technique, which consists in determining the speed of the particles knowing that it is proportional to the rate of fluctuation of the intensity signal, is used.

A.3 Scanning Electron Microscopy (SEM) and Energy Dispersive Spectroscopy (EDS)

Scanning electron microscopy (SEM) is a technique which consists in the obtainment of various signals by means of accelerated electrons that interact with a solid sample. The kinetic energy of the electrons is dissipated and, consequently, produces diverse signals (which include secondary electrons, backscattered electrons, photons (characteristic x-rays), visible light and heat) that reveal information about the sample. Signals from secondary electrons are used for image generation and for showing the morphology and topography of the samples.

On the other hand, x-ray generation, produced by inelastic collisions of the incident electrons with electrons in discrete orbitals of atoms in the sample, is useful for elemental analysis [51]. An energy dispersive detector is used to separate the characteristic x-rays of different elements into an energy spectrum and, posteriorly, an EDS system software analyses it in order to determine the abundance of specific elements [52].

A.4 Nitrogen Adsorption

Nitrogen adsorption is used to measure the specific surface area of a material. A plot of the volume of nitrogen (N_2) adsorbed as a function of the relative pressure is obtained and can be used to calculate the surface area by means of the BET (Brunauer-Emmett-Teller) model. This model is an extended version from Langmuir's model and can be represented, in its linearized form, by:

$$\frac{P/P_0}{V^a(1-P/P_0)} = \frac{1}{V_m^a C_{BET}} + \frac{C_{BET}-1}{V_m^a C_{BET}}\frac{P}{P_0} \quad \text{(A.1)}$$

Where P is the pressure, P_0 the maximum pressure used, V^a the adsorbed volume of nitrogen, V_m^a the volumetric capacity of the monolayer and C_{BET} a parameter of the model that is proportional to the exponential of the difference between the adsorption heat of the first layer and the adsorption heat of the following layers. Posteriorly, the BET surface area, S_{BET}, can be calculated by:

$$S_{BET} = n_m^a N_A a_m \quad \text{(A.2)}$$

Where n_m^a is the monolayer capacity (number of moles of molecules that completely cover the surface – monolayer) and a_m a parameter that represents the area occupied by each molecule. For nitrogen at -196 ºC this parameter takes the value of 0.162 nm^2.

A.5 Fourier-Transform Infrared Spectroscopy (FTIR)

Infrared spectroscopy is a technique based on the fact that molecules absorb frequencies that are characteristic of their structure. When infrared radiation passes through a sample, some radiation is absorbed by it and some is transmitted (passes through it). An infrared spectrum is obtained by determining the fraction of incident radiation that is absorbed at a particular energy [53].

In an FTIR equipment, the source emits radiation that is guided through an interferometer and then to the sample. An interferometer is an apparatus that splits the light from a single source into two beams that travel different optical paths and then combines them again to produce an interference that gives information about the difference in optical path lengths. Also, a moving mirror alters the distribution of infrared light that passes to the interferometer and the signal is recorded as a function of the change of pathlength between the two beams. At last, Fourier transformation can be used to turn into this raw data into the sample's spectrum [53].

It should be noted that, most usually, this type of analyses is performed in order to determine the functional groups present in a compound. However, in this case, it is intended to distinguish between the several types of polymorphs that calcium carbonate can form. This can be achieved by direct comparison with FTIR spectras found in literature - Figure 26.

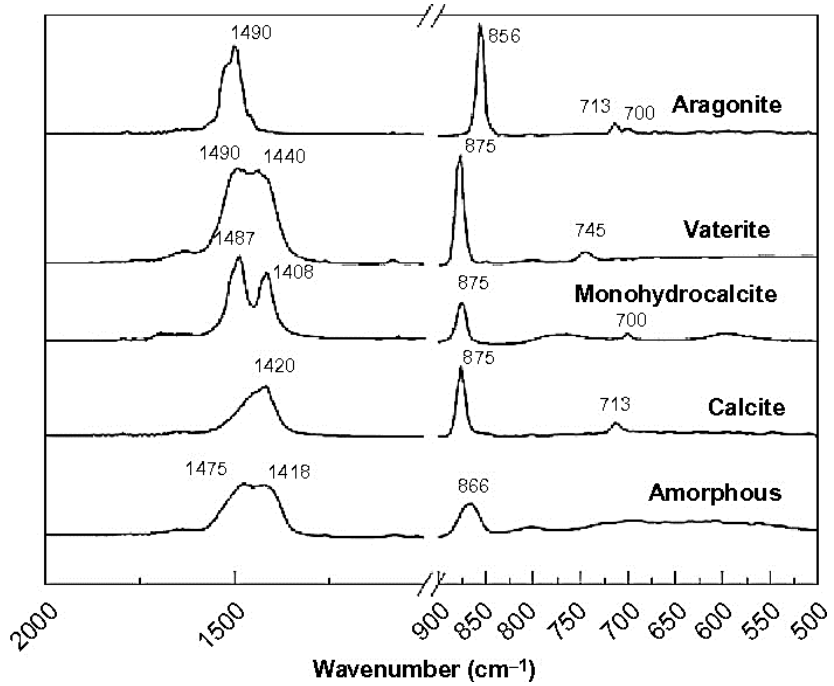

Figure 26 - FTIR spectra for the different forms of calcium carbonate [54].

A.6 Transmission Electron Microscopy (TEM)

The transmission electron microscope (TEM) is a type of microscope in which a beam of electrons is transmitted through an ultra-thin specimen generating, consequently, a tremendous range of signals that allow the obtainment of, among others, images and diffraction patterns (DP).

TEM DP contain information on the crystal structure, lattice repeat distance and the specimen shape and are especially useful for material scientists and nanotechnologists for whom crystal structure is an essential characteristic when it comes to controlling properties [55].

Appendix B. TEM Analysis

The tables below present the data of the fringe spacings and angles for the three polymorphic forms of calcium carbonate and for different crystallographic directions (h', k and ℓ).

Table 11 - Fringe spacings and angles of calcite for different crystallographic directions.

2θ / °	δ / Å	Intensity	h'	k	ℓ
23.0218	3.860000	12	0	1	2
29.4049	3.035000	100	1	0	4
31.4176	**2.845000**	**3**	**0**	**0**	**6**
35.9654	**2.495000**	**14**	**1**	**1**	**0**
39.4009	2.285000	18	1	1	3
43.1447	2.095000	18	2	0	2
47.1226	1.927000	5	0	2	4
47.4886	1.913000	17	0	1	8
48.5122	1.875000	17	1	1	6
56.5530	1.626000	4	2	1	1
57.4001	1.604000	8	1	2	2
58.0733	1.587000	2	1	0	10
60.6762	1.525000	5	2	1	4

Table 12 - Fringe spacings and angles of vaterite for different crystallographic directions.

2θ / °	δ / Å	Intensity	h'	k	ℓ
20.9420	4.238410	81	0	0	2
24.9040	3.572370	448	1	0	0
27.0630	3.292080	940	1	0	1
32.7580	2.731590	999	1	0	2
40.6771	2.216210	86	1	0	3
42.6269	2.119240	120	0	0	4
43.8581	2.062560	690	1	1	0
49.0811	1.854590	291	1	1	2
49.9999	1.822640	801	1	0	4
51.0919	1.786220	46	2	0	0
52.2979	1.747830	15	2	0	1
55.8050	1.646010	267	2	0	2
61.3512	1.509830	32	2	0	3

Table 13 - Fringe spacings and angles of aragonite for different crystallographic directions.

2θ / °	δ / Å	Intensity	h'	k	ℓ
21.0748	4.212000	3	1	1	0
22.2959	3.984000	1	0	2	0
26.2120	3.397000	100	1	1	1
27.2153	3.274000	50	0	2	1
31.1148	**2.872000**	**6**	**0**	**0**	**2**
32.7406	2.733000	9	1	2	1
33.1270	2.702000	60	0	1	2
36.1753	**2.481000**	**40**	**2**	**0**	**0**
37.2636	**2.411000**	**14**	**0**	**3**	**1**
37.8829	2.373000	45	1	1	2
38.4039	2.342000	25	1	3	0
38.6095	2.330000	25	0	2	2
41.1858	2.190000	12	2	1	1
41.6231	2.168000	2	1	3	1
42.8654	2.108000	20m	1	2	2
42.8654	2.108000	m	2	2	0
45.8520	1.977400	55	2	2	1
46.5339	1.950000	1	0	3	2
48.3175	1.882100	25	0	4	1
48.4435	1.877500	25	2	0	2
48.8842	1.861600	2	0	1	3
49.8579	1.827500	4	2	1	2
50.2279	1.814900	20	1	3	2

At last and as mentioned, more images of the samples submitted to TEM analysis with the respective fringe spacing measurements are presented below from Figure 27 to Figure 30.

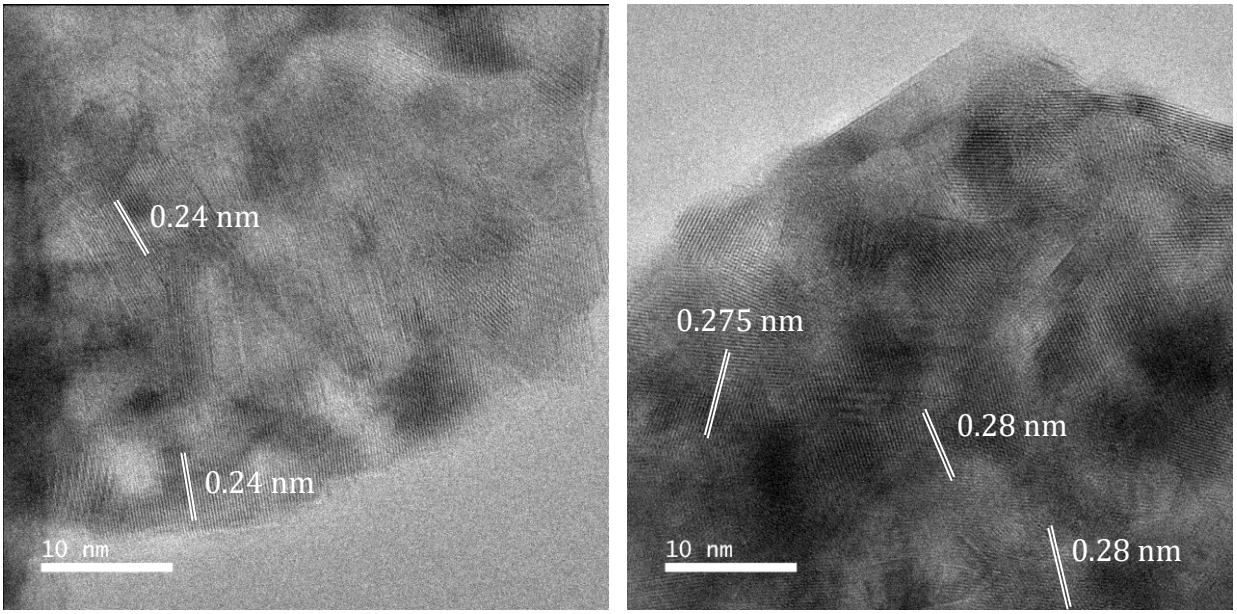

Figure 27 - TEM images of sample B1 with the respective fringe measurements.

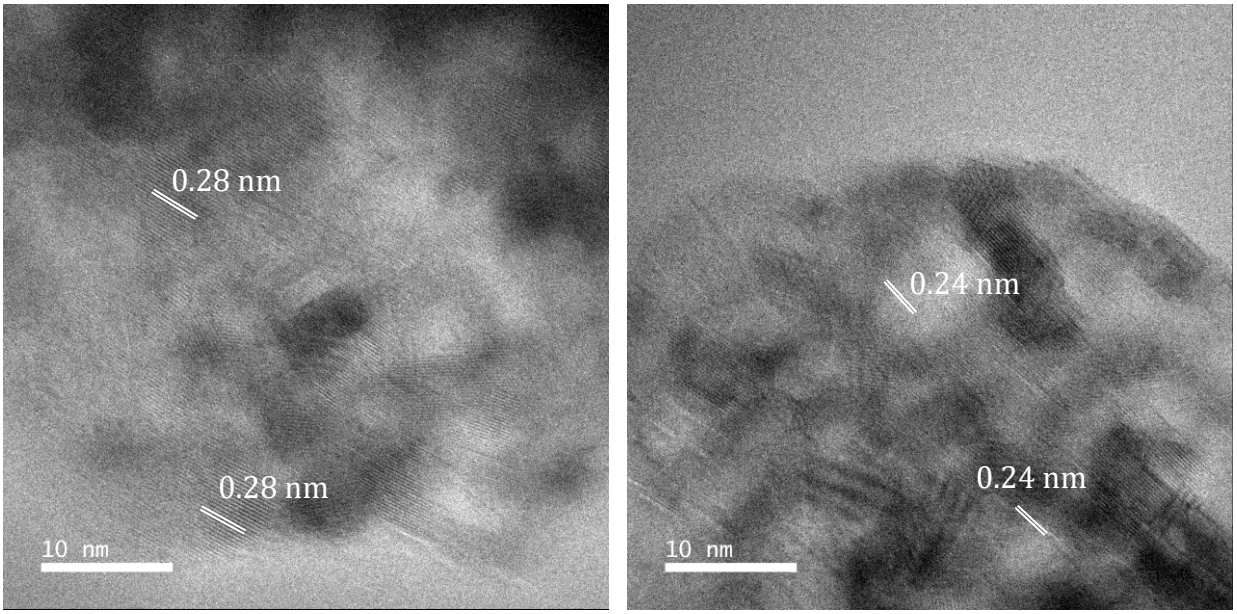

Figure 28 - TEM images of sample N04 with the respective fringe measurements.

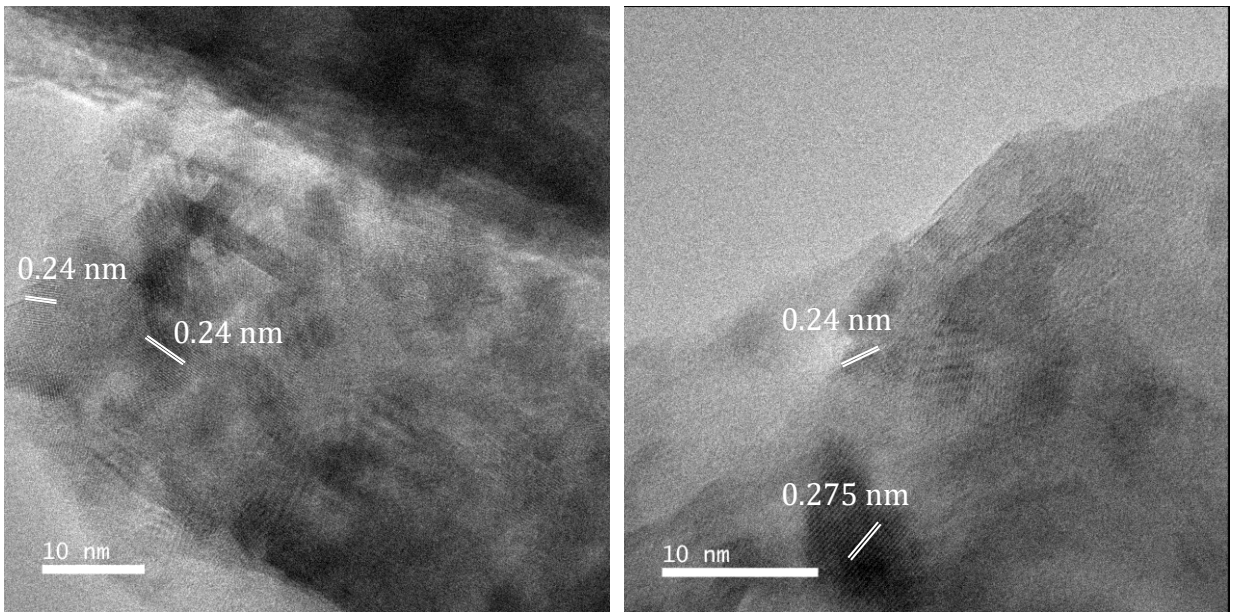

Figure 29 - TEM images of sample N09 with the respective fringe measurements.

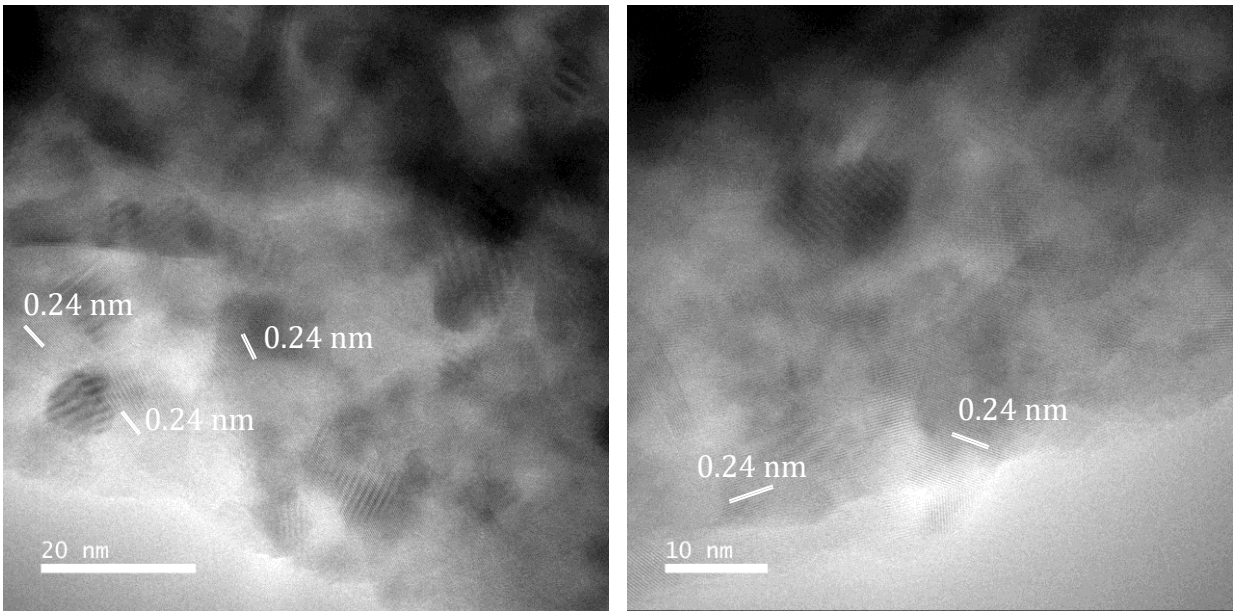

Figure 30 - TEM images of sample N13 with the respective fringe measurements.

Appendix C. Economic Analysis

The figure below shows the process that was simulated in Aspen Plus to its full detail.

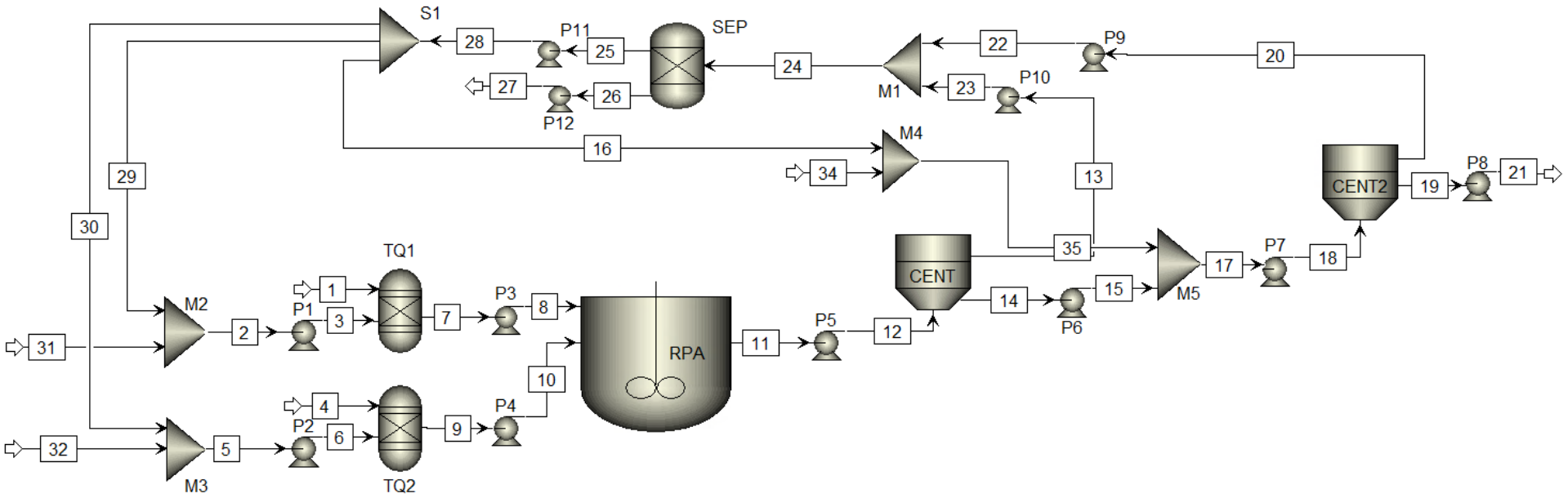

Figure 31 - Detailed flowsheet of the process simulated in Aspen Plus.

The composition in terms of the compounds' mass flow rate, Q, for the more important streams of the process is presented in Table 14. It should be noted that the streams designation is in accord with Figure 31.

Table 14 - Composition of the more relevant streams of the process.

Stream	Q / kg·h^{-1}				
	$CaCl_2$	K_2CO_3	H_2O	$CaCO_3$	KCl
7	123	-	5 535	-	4.1
9	-	153	5 535	-	4.1
11	0.08	0.06	11 071	111	173
14	0.08	0.06	519	105	8.1
21	0.08	0.05	496	100	4.1
13	0.004	0.003	10 552	5.5	165
20	0.004	0.003	522	5.3	4.3
34	-	-	69	-	-
29	-	-	4 768	-	4.1
30	-	-	4 768	-	4.1
16	-	-	431	-	0.4
27	0.008	0.006	1 107	11	161
31	-	-	767	-	-
32	-	-	767	-	-

Furthermore, and now relative to the sizing of the equipment, it was assumed a storage capacity of 15 days in the sizing of the product's storage tank. For the water, the storage tank volume was estimated as three times the volume of the recycling water of the process.

The volume of the equipment and their respective dimensions calculated by APEA are presented in the table below.

Table 15 - Specifications of the equipment.

Equipment	Corresponding Block	V / m^3	D / m	L / m
Stirring tank	TQ1	0.9	0.6	3.0
	TQ2	0.9	0.6	3.0
	RPA	2.8×10^{-2}	0.2	1.5
Centrifuge	CENT and CENT2	-	0.5	1.0
Storage tank for $CaCO_3$ suspension	-	56.2	2.9	8.5
Storage tank for water	-	32.7	2.4	7.0

Table 16 discriminates the capital costs into several categories.

Table 16 – Detailed capital costs.

Description	Cost / €
Purchased equipment	1 028 257
Equipment Setting	15 772
Piping	610 611
Civil	85 309
Steel	54 230
Instrumentation	1 327 818
Electrical	1 261 837
Insulation	70 466
Paint	2 338
Other	1 822 149
G and A overheads	144 752
Contract fee	287 140
Contingencies	1 207 921